UNIVERSITÀ
DI PAVIA

Dipartimento di Biologia e Biotecnologie
"Lazzaro Spallanzani"

Laurea Magistralis in Molecular Biology and Genetics

Effects of 1nM cypermethrin exposure on in vitro preimplantation mouse embryo development

Supervisor:
Valeria Merico

Experimental thesis by
Elisa Sotgiu

Academic Year
2025/2026

ABSTRACT

Cypermethrin (CYP) is a synthetic pyrethroid insecticide widely used in agriculture. Due to its extensive application, CYP has become one of the major environmental pollutants worldwide. It is well established that CYP, entered into the body via contaminated food and water consumption or lipophilic absorption, exerts toxic effects in mammals and aquatic organisms. While the toxicological impact of CYP on adult tissues and gonads is well documented, its effects on preimplantation embryo development remains largely unexplored. The aim of this thesis is to address this gap by evaluating CYP-induced alterations on preimplantation embryo development rate and assessing the quality of treated blastocyst, both morphological and molecular perspectives.

Embryos were generated via *in vitro* fertilization and assigned to two experimental groups: a control group (CTR), cultured under physiological laboratory conditions, and treated group (CYP), exposed to 1 nM CYP in developmental culture starting 3 hours post-insemination.

The results demonstrated that CYP significantly decreases preimplantation embryo development rates across all evaluated checkpoints, including 2-cell, 4-cell, morula and blastocyst stages; Furthermore, CYP-treated embryos that reach blastocyst stage exhibit reduced quality compared to CTR, characterised by a lower total number of cells and a markedly higher cell death rate. This increase in apoptosis was observed globally as well as within the inner cell mass and trophectoderm lineages individually. Consistently with these morphological findings, microarray combined to bioinformatic analyses revealed that CYP alters blastocyst transcriptome, disrupting key regulators of metabolic pathways, cell cycle control, the oxidative response, cell differentiation, and pluripotency maintenance. These molecular alterations likely compromise the developmental competence of surviving blastomeres, impairing the expansion process and ultimately reducing overall developmental yields.

Taken together, these findings demonstrate that environmental exposure to CYP during the preimplantation window compromises both the developmental competence and molecular integrity of mouse embryos.

Future prospectives will focus on:

- Stage-specific transcriptomics: Analyzing early and expanded blastocysts separately to isolate the drivers of expansion failure.
- Protein validation: Quantifying key targets (e.g., via Western blot/IF) to confirm that mRNA alterations manifest at the protein level.
- In vivo functional assays: Performing embryo transfers in mice to evaluate the impact of CYP exposure on implantation and post-implantation development.

RIASSUNTO

La cipermetrina (CYP) è un insetticida appartenente alla famiglia dei piretroidi e negli anni, a causa del suo massivo utilizzo, è diventata uno dei maggiori inquinanti ambientali al mondo. In letteratura, è noto che l'insetticida, introdotto nell'organismo attraverso l'assunzione di acqua e cibo contaminati o tramite assorbimento lipofilo, esercita effetti tossici nei mammiferi e nei pesci. In particolare, l'azione della CYP sui tessuti dell'organismo umano adulto e sulle gonadi è ben caratterizzata, ma gli effetti dell'insetticida sullo sviluppo embrionale preimpianto rimangono ancora poco noti.

Lo scopo della mia tesi è colmare questa lacuna di conoscenze, valutando le alterazioni indotte dalla CYP sul tasso di sviluppo embrionale in fase di preimpianto e sulla qualità della blastocisti, sia dal punto di vista morfologico che molecolare.

Gli embrioni utilizzati negli esperimenti sono stati ottenuti mediante tecnica di fecondazione *in vitro* (IVF) e, per ciascuna analisi, sono stati considerati un gruppo di controllo (CTR) coltivato in condizioni fisiologiche di laboratorio e un gruppo trattato (CYP), che indica embrioni coltivati, per tutto lo sviluppo embrionale, in presenza di 1 nM di CYP a partire 3 ore post-inseminazione.

I risultati ottenuti mostrano che la CYP riduce significativamente i tassi di sviluppo embrionale in fase preimpianto in tutti i checkpoint considerati per la valutazione, a partire dallo stadio di embrione a 2 cellule, 4 cellule, morula e blastocisti. Gli embrioni del gruppo CYP che raggiungono lo stadio di blastocisti, inoltre, presentano un numero totale di blastomeri significativamente minore rispetto a quelli di CTR e sono caratterizzati da un tasso di morte cellulare significativamente più elevato, senza mostrare diversa localizzazione se si considerano le due linee differenziative di massa cellulare interna e trofectoderma.

Inoltre, una successiva analisi tramite microarray combinata ad un'analisi bioinformatica ha messo in evidenza che la CYP altera il trascrittoma della blastocisti trattate e influenza l'espressione di regolatori chiave delle vie metaboliche, del controllo del ciclo cellulare, della risposta ossidativa, del differenziamento cellulare e delle vie di mantenimento della pluripotenza.

Nel complesso, questi risultati dimostrano che un'esposizione a 1 nM di CYP durante la finestra di sviluppo embrionale preimpianto compromette la competenza dello sviluppo sia l'integrità molecolare degli embrioni murini.

Le prospettive future si concentreranno su:

- Trascrittomica stadio-specifica: Analizzando separatamente le blastocisti a momenti diversi di sviluppo (precoci o espanse) per isolare il time di alterazione dei fattori molecolari che risultano essere deregolati.

- Validazione proteica: quantificando i bersagli chiave (es. tramite Western blot o immunofluorescenza) per confermare che le alterazioni dell'mRNA si riflettano a livello proteico.
- Saggi funzionali in vivo: eseguendo un trasferimento embrionale in modelli murini per valutare l'impatto dell'esposizione a CYP sull'impianto e sullo sviluppo post-impianto.

CONTENTS

1. INTRODUCTION

1.1 Insecticides classification and cypermethrin diffusion

Pesticides refer to any substance or combination of substances intended for preventing, destroying, or controlling any pest *(Food and Agriculture Organization of the United Nations, 2002*); thus, they are compounds designed to protect crops from insect, diseases and weeds *(Ahmadi et al, 2024).*

In the last century, their usage has increased exponentially to allow agricultural expansion while maintaining food security for the growing population *(Tudi et al, 2021; Sinha and Shrivastava, 2024)*. The massive usage of pesticides has caused their entry into the ecosystem through various routes, ultimately altering environmental balance. As shown in Figure 1.1.1, these compounds accumulate in agricultural crops and long-distance dispersion occurs via soil, water and air. Consequently, pesticides are among the major pollutants in ecosystem *(Kalyabina et al 2021).*

Depending on the target organism, pesticides are categorized in different groups: i) herbicides are molecules directed against weeds; ii) fungicides are used to control mold and fungal growth; iii) rodenticides include anticoagulants and strychnine that kill rodents; iv) insecticides exert toxic effects on insects. Among these categories, insecticides are the fastest-acting and most hazardous *(Sinha and Shrivastava, 2024)*. The toxicity of these molecules is determined by considering environmental exposure factor, formulation and concentration *(Prasamthi et al, 2005).*

Insecticides comprise of natural compounds, derived from plants and mineral oils, or synthetic compounds. The most widely used synthetic insecticides are classified based on their chemical structure, with the main groups being carbamates, organochlorines, organophosphates and pyrethroids *(Saka et al 2011),* which can be further divided in Type I and Type II classes. Class I components, also named non-cyanopyrethroids, lack a cyano group in their chemical structure. They exhibit rapid action by binding to and inactivating sodium channels. Conversely, Type II pyrethroids are characterized by the presence of an alpha-cyano group that stabilizes sodium channel in an open state, inducing a prolonged depolarization of neuronal cell membranes *(Soderlund et al, 2002).*

All synthetic pyrethroids are derived from pyrethrins, which are natural compounds extracted from *Chrysantemum Cinerariifolium (Ullah et al, 2019).* Of all possible molecules synthetized, the Word Health Organization (WHO) has approved the use of only permethrin, deltamethrin and cypermethrin (CYP) which are Type I, Type II and Type II pyrethroids, respectively *(WHO, 2017; European Union Directive, 2009)*. Among these compounds, CYP is the most widely used because of its low cost and its rapid degradation via photolysis on illuminated surfaces *(Arikan et al, 2026).* The insecticide is usually sprayed onto crop surface, where it exerts its function *(Cardoso et al, 2021; Li et al, 2024)*. Due to its massive usage, CYP has contaminated the environment and is now considered one of the

principal pesticides associated to human health risks *(Soderlund et al 2002).* The insecticide can easily reach the soil through rainfall, which transports it from the leaf surfaces to the ground. Once there, CYP strongly binds the organic matter present *(Ismail et al, 2013),* decreasing its bioavailability and slowing its degradation rate *(European Food Safety Authority, 2008; Schreinemachers et al, 2017*). Generally, in oxygen-limited environment, CYP can persist for weeks to months due to the chronic exposure leading to molecule accumulation *(Gan et al, 2005; Kansal et al., 2023).* Insecticide present in the soil can be absorbed by edible vegetation, entering the food chain *(Silva et al, 2008).*

CYP also reaches aquatic environment via atmospheric precipitation and waterways (*Governmnent of India, 2020*), with high concentrations often detected in surface water (*Jaensson et al, 2007*). In this context, the high absorption rate driven by insecticide's lipophilicity (*Fetoui et al, 2010*) facilitates its accumulation in fish, leading to bioaccumulation in edible tissues (*De Gavelle et al, 2016*). Currently, environmental levels of CYP in water bodies frequently exceeds regulatory safety limits (*Sinha and Shrivastava, 2024*).

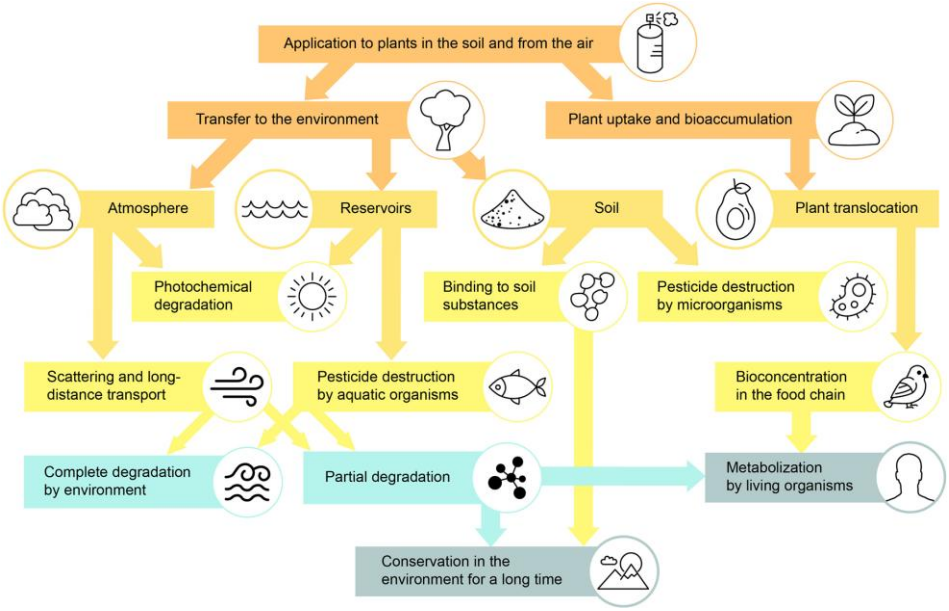

Figure 1.1.1 *Routes of CYP diffusion in the environment (Kalyabina et al, 2021)*

1.2 CYP toxicity among vertebrates

Due to its widespread application, the adverse effects of CYP have been documented across numerous aquatic and terrestrial species, impacting multiple physiological systems. Among these, neurotoxicity is the most extensively investigated, as voltage-gated sodium channels in neuronal membrane represent the primary target of this insecticide *(Sinha and Shrivastava, 2024).* Specifically, CYP bind to sodium channels and delays their inactivation, thereby maintaining a prolonged open state that leads to cellular hyperexcitation and hypopolarization and altering signal transmission *(Clark and Symington, 2012; Sinha and Shrivastava, 2024)*. Beyond this primary mechanism of action, CYP

metabolism generates cyanohydrin intermediates, which subsequently decompose into aldehydes and cyanides, driving the intercellular generation of reactive oxygen species (ROS) *(Wielgomas and Krechniak, 2007).* Elevated ROS levels trigger intracellular calcium overload and induce lipid peroxidation (LPO), ultimately causing cytotoxicity and genotoxicity *(Sinha and Shrivastava, 2024).* Indeed, Promthep et al. (2022) demonstrated that exposure to CYP in human SH-SY5Y neuroblastoma cells induces G0/G1 cell cycle arrest, fragmentation of DNA at sub-G0 phase and a higher number of cells that expresses galactosidase marker for senescence. CYP induces DNA damage and apoptosis *(Promthep et al, 2022).* The oxidative stress response following pyrethroid exposure has also been evaluated in rat brain, where early postnatal life is characterized by an initial upregulation of catalase (CAT), glutathione (GSH) and superoxide dismutase (SOD). These three genes undergo a decrease in expression during rat development, resulting in a marked downregulation in the adult animal. The weakened antioxidant defence system cannot compensate for the damage induced by ROS, leading to persistent oxidative stress *(Elsawy et al, 2017).* Within the central nervous system, CYP also induces nigrostriatal dopaminergic neurodegeneration by altering mitochondrial proteome, leading to organellar dysfunction *(Agrawal et al, 2015).* Exhibiting high lipophilicity, it readily undergoes bioaccumulation throughout body tissues *(Clark and Symington, 2012)* extending these cytotoxic effects to other organ systems. In the liver of Wistar rat treated with different doses of CYP for 15 days, expression levels of GSH, CAT and SOD were downregulated *(Kašuba et al, 2022)* and the same results were reported in albino rat models *(Abdou et al, 2019)*. In *Clarians Gariepinus,* CYP exposure induces enlarged liver, hepatocyte and nuclear ageing, tissue vacuolization and haemorrhage *(Agbohessi et al, 2023)*.

CYP also plays a role in kidney impairment: *O. Niloticus* displays thickening of Bowman capsule, globular shrinkage and necrosis of renal tubules when treated with dosage of CYP between 1,25 and 2,5 g/L and dilatation of lumen, hyaline degradation of tubular epithelium tissues and cytoplasmatic vacuolation with 2.5 g/L CYP administration *(Majumder and Kaviraj, 2022)*. Simulating chronic exposure to CYP for 45 days in *Catla catla* reduces CAT, SOD, GSH, Glutathione S-transferases (GST) expression, while LPO levels remain throughout the exposure window *(Sharma et al, 2021)*. From an immunological perspective, CYP reduces the leukocytes ratio favouring neutrophils one in carp *(Soltanian et al, 2017*). In mice, CYP induces spleen toxicity by increasing LPO, Hydrogen peroxide (H2O2), Nitric Oxide (NO) levels and reducing weight of the organ and GSH and SOD expression *(Namdev et al, 2023)* and alters haematological physiology in *Oncorhyncus mykiss* increasing the total amount of protein in serum, particularly albumin and globulin, and increasing Ig and proteases levels in blood *(Naserabad et al, 2024)*.

1.3 CYP and reproductive toxicity in mammals

Recently, a concerning correlation between CYP exposure and impaired mammalian fertility has emerged. Data suggest that the insecticide negatively impacts both male and female reproductive systems at doses below those required to induce overt neurotoxicity *(Marettova et al, 2017)*. Although CYP is not officially classified as a reproductive or developmental toxicant *(Environmental Protection Agency, 2009)*, its widespread agricultural and residential use facilitated off-target toxicity. Indeed, repeated oral administration induces mild to moderate toxic symptoms in both male and female rats *(Marettova et al, 2017).*

In female rats, CYP toxicity affects both ovary and uterus in a dose-dependent manner. Exposure to 20mg/ kg/ day results in a significant loss of follicular cells and oocyte inside the ovary *(Grewal et al, 2010)*. Increased the dosage to 40 mg/ kg/ day leads to reduced ovarian weight, increased thickness of myometrum, greater length and weight of uterus, elevated follicular atresia, and depleted ovarian levels of phospholipids, lipids, cholesterol and proteins. At the biochemical level, CYP-treated rat ovaries exhibit increased alkaline phosphatase activity alongside decreased lactate dehydrogenase compared to control *(Sangha et al, 2013*). *In vitro* studies on bovine luteal cells (LCs) further confirm the severe cytotoxic impact of CYP, which markedly reduces progesterone secretion into the culture medium. Moreover, LCs exposed to varying CYP concentrations and timeframes show clear signs of necrosis, vacuolation and loss of cells viability *(Gill et al, 2011)*. In Holstein dairy cows, CYP exposure induces endometrial glandular atrophy in uterus *(Garoussi et al, 2010).* Similarly, intraperitoneal administration of CYP (25/ 50/ 75 mg/kg body weight) in rabbit induces prominent histopathological changes in both uterine and ovarian tissues *(Ullah et al., 2006)*. In the uterus, CYP disrupts adenosine triphosphate pathway, leading to glandular atrophy, tissue stiffening driven by connective cells proliferation and vascular congestion. In ovary, higher doses of the pyrethroid induce connective tissue proliferation in the cortex, while significant alterations in corpora luteal occur across all tested doses *(Ullah et al, 2006).*

In pig oocyte, CYP treatment impairs both nuclear and cytoplasmatic maturation by inducing chromosomal aberrations and affecting mitochondrial integrity, cortical granules and endoplasmic reticulum (ER). Consequently, the rate of oocyte maturation decreases in a dose-dependent manner. Furthermore, downregulation of redox genes expression drives ROS accumulation and depletion of intracellular GSH *(He et al, 2023)*. Additionally, CYP induces DNA damage and disrupted ER function in pig oocyte by altering the expression of key genes involved in DNA damage repair and ER stress response *(Sun et al, 2023).*

Several pyrethroids exhibit endocrine disrupting activity by interfering with physiological hormonal signalling *(Marettova et al, 2017).* In this context, both *in vivo* and *in vitro* studies have investigated

CYP's role as endocrine disruptor, contradictory results likely attributable to differences in assay sensitivity and experimental design *(Brander et al, 2012)*. Nevertheless, CYP consistently exhibits hormonal activity, mimicking estrogenic asset *in vitro (Chen et al, 2002)* while exerting anti-estrogenic effects *in vivo (Gill et al, 2009)*. Estrogenic activity was demonstrated by using p2 mRNA expression assay, where CYP induced p2 transcript levels with lower potency than permethrin but higher potency than deltamethrin *(Chen et al, 2002)*. Conversely, direct interaction between CYP and estrogen receptors has been reported in both rats and human models, providing a mechanism for its anti-estrogenic properties *(Sun et al, 2014).*

Regarding male fertility, the effects of CYP have been extensively evaluated in mouse Sertoli cells (TM4). Given their indispensable role in the testis development, blood-testis barrier integrity, and spermatogenesis *(Ni et al, 2019)*. CYP treatment reduces cell survival rate *(Wang et al, 2020)* and triggers apoptosis via mitochondrial Ca2+ overload, driven by the upregulation of cleaved caspase3 (Casp3) and cleaved poly ADP-ribose isomerase (PARP) *(Zhang et al, 2024)*.

Specifically, CYP upregulates the IP3R1–GRP75–VDAC1 axis, a critical signalling pathway governing ER-mitochondrial coupling. Inositol 1,4,5-trisphosphate receptor type 1 (IP3R1) is an ER-resident Ca^{2+} channel physically coupled to voltage-dependent anion channel 1 (VDAC1) on the outer mitochondrial membrane via the chaperone glucose-regulated protein 75 (GRP75) *(Thoudam et al, 2019).*

This macromolecular complex facilitates direct Ca^{2+} transfer from the ER to the mitochondrial matrix. By upregulating all key protein components of this pathway, CYP promotes an excessive mitochondrial calcium influx that triggers the opening of mitochondrial permeability transition pore. Consequently, pro-apoptotic factors are released, inducing TM4 programmed cell death *(Marchi et al, 2018)*. These signal cascades promote the cleavage of Casp3, which subsequently cleaves PARP, leading its inactivation *(Choudhary et al, 2015)*. As a results, single strand DNA nicks can no longer be repaired, committing TM4 cells to apoptosis *(Zuo et al, 2014).*

Because Sertoli cells loss directly impairs germ cell support, CYP-induced TM4 apoptosis serves as a primary driver of male reproductive toxicity *(Zhang et al, 2024)*.

Although pyrethroid toxicity in adult vertebrate tissues has been extensively characterized at both anatomical and molecular levels, the specific impact of cypermethrin on early preimplantation development remains largely unexplored.

1.4 Preimplantation development

Fertilisation of an ovulated oocyte by capacitated sperm within the oviduct results in the formation of a zygote. The defining feature of the zygote is totipotency, the capacity of a single cell to

differentiate in both embryonic and extraembryonic lineages. Throughout preimplantation development, the embryo undergoes a series of cleavage divisions characterized by S and M phases, bypassing the G1 and G2 phases. Consequently, these reductive cleavage divisions generate progressively smaller daughter cells, eventually scaling down toward typical somatic cell dimensions *(Schulz and Harrison, 2019).*

The initial stages of preimplantation development are directed by approximately 40 transcripts called maternal effect factors (MEFs). These maternal mRNAs and proteins are synthesized and stored by the oocyte during oogenesis; notably, several are related to SWI/SNF, ISWI, CHD and INO80 chromatin-remodelling families *(Cabot and Cabot, 2018)*. In the mouse embryo, the maternal-to-zygotic transition occurs between the 2-cell and 4-cell stages, characterized by the progressive degradation of MEFs tightly coordinated with the transcriptional activation of zygotic genome *(Tadros and Lipshitz, 2009).* Beyond this developmental threshold, subsequent cell divisions are governed entirely by zygotic gene products.

At 8-cell stage, a process called compaction initiates; blastomeres begin to adhere to one to another via E-Cadherin (E-Cad), culminating in the establishment of adherent junctions along their basolateral membranes. Compaction generates an increase in blastomere surface tension given by actomyosin cortex contraction, which is partially compensate by cell-cell adhesion forces *(Maître et al, 2017)*. E-Cad also plays a subtle role in driving compaction by redirecting myosin-2 distribution *(Pfeffer, 2020)*. From 8-cell to 16-cell, compact morula architecture is further stabilized by the extension of apical surface filopodia between blastomeres *(Fierro-González et al, 2013).*

Approximately one hour after compaction onset *(Zhu et al, 2017)*, cells acquire spatial asymmetric phenotype via cell polarization. The precise timing of polarization is governed by the expression of key transcription factors, namely TEA domain 4 (TEAD4) or AP2 gamma (Tfap2c) *(Zhu et al, 2020)*. Both factors regulate genes governing actin dynamics; specifically, Tfap2c promotes the transcription of Rock1/2, which direct cytoskeleton reorganization *(Cao et al, 2015)*. Microfilaments remodelling is therefore central to cell polarization.

Polarization initiates with a gradual accumulation of activated myosin-2 and actin in the cortex localized under contact-free blastomere surface *(Maître et al, 2015; Zhu et al., 2017).* This is accompanied by a thickening of actin meshwork triggered by phospholipase C (PLC) signalling. Activated PLC splits phosphatidylinositol 4,5-bisphosphate (PIP2) into inositol 1,4,5-trisphosphate (IP3) and diacylglycerol (DAG) which remains in membrane compartment where it activates canonical protein C kinase (PKC). This kinase recruits RhoA, which subsequently promotes myosin regulatory light chain (RLC) phosphorylation. This modification on RLC allows myosin-2 assembly and accumulation at the apical cortex *(Zhu et al, 2017).*

By the mid 8-cell stage, *de novo* apical polarization pathway proceeds, with the accumulation of polarity proteins ezrin and PARD6 near the centre of contact-free exposed region of blastomeres *(Zhu et al, 2017)*. The physical size of apical domain is determined by the balance between positive stimulus for domain enlargement and systems that inhibits it. On one hand, Ezrin engages in a positive feedback loop that promotes its own accumulation and, as an actin-membrane crosslinker, drives apical expansion. On the other hand, the limited availability of plasma membrane binding sites (such as PIP2) and RhoA-mediated restrictions on Ezrin mobility constrain domain enlargement *(Zhu et al, 2020).*

Apical domain localisation depends on mechanical contacts positioning between blastomeres and becomes definitive when Ezrin and PARD6 enrichment *(Vinot et al, 2005)*.

At late 8-cell stage, the actomyosin framework changes its conformation, undergoing thickening on the edges of expanding apical domain and thinning underneath it. This transition defines the actomyosin ring *(Zhu et al, 2017)*. Following ring assembly, PARD6B within the apical domain, attracts and activated aPKC *(Vinot et al, 2005; Alarcon, 2010)*. Active aPKC performs three principal functions: i) maintenance of cell polarity by excluding basolateral proteins, such as PAR1, to basolateral cortex (Buckley and St Johnston, 2022); ii) stabilization of F-actin filament by maintaining Ezrin phosphorylation required for the interaction Ezrin-cytoskeleton binding *(Liu et al, 2013); iii)* guidance of cell toward asymmetric (radial) division together with the microtubule organising center (MOC) *(Pfeffer, 2024).*

Because the apical domain is less contractile than the surrounding F-actin enriched actomyosin ring reinforced, external blastomeres become resistant to cell internalisation. In this conformation, all blastomeres are polarized, with polarised surface exposed to the external environment *(Pfeffer, 2024)*. Division planes can theoretically orient symmetrically (parallel to the apicobasal axis) or asymmetrically (perpendicular to the apicobasal axis). Symmetrical division generates two polar daughter cells, both destined to remain on the embryo's outer surface. Asymmetrical division yields one polar daughter cell (inheriting both apical and basolateral domains) and one apolar daughter cell, which is directed inward. In practice, most cleavage planes adopt intermediate angles relative to the apicobasal axis *(Watanabe et al, 2014);* as a result, daughter cells inherit a variable amount of the apical domain, which ultimately determines their positioning *(Anani et al, 2014)*. This repositioning depends on both the presence or absence of an apical domain of an apical domain *(Pfeffer, 2024)* and the cell surface tension, which is dictated by cytoplasmic volume and is lower in internalized blastomeres *(Pomp et al, 2022)*. These divisions lead to 16-cell compact morula formation containing less than 5 blastomeres fully internalized and the other facing the outside *(Anani et al, 2014)*. At this developmental stage, a shift from asymmetrically to symmetrically cell division tendence is recorded

(Watanabe et al, 2014). This transition is driven by tension-induced changes in outer cell morphology that reposition of spindle orientation *(Dumollard et al, 2017).* Regarding the apical domain, it is inherited by outer blastomeres following cytokinesis; subsequently, the polarity proteins PARD6 and Ezrin relocalize from the apical area toward the periphery, forming the apical ring *(Zenker et al, 2018)*. Concurrently, increasing hydrostatic pressure generated by the new cell shape, drives outer actin ring expansion toward cell-cell junction until. By the 16-to-32 cell stage, adjacent actin rings seal together via a myosin-2 dependent "zipper-like" mechanism *(Zenker et al, 2018)*, forming a physical barrier that also controls fluid exchange with external environment. As embryonic development proceeds, from 32 cells outward, massive changes in embryo osmosis occurs. Specifically, Na+/K+-ATPase of blastomere's basolateral area *(Watson et al, 2004)* and Na+/H+ cotransporter (NHE-3) at the apical side *(Kawagishi et al, 2004)*, establish and maintain an osmotic ion gradient in between outside and inside the embryo *(Madan et al, 2007)*. This gradient generates a massive water influx, supported by aquaporins activity *(Barcroft et al, 2003),* that rapidly increases the internal embryo pressure. Weaker E-cad mediated adhesions connecting two blastomeres start to break, forming a "bubbles"-like cavity filled of water between the cells. Usually, these junctions are placed in basolateral domains *(Kim and Bedzhov, 2022; Le Verge-Serandour et al ,2022).* These small fluid pockets progressively coalesce into a single, large internal cavity: the blastocoel. The formation of the blastocoel transforms the morula into a blastocyst and establishes its primary developmental axis, segregating the embryo into embryonic and abembryonic poles *(Kim and Bedzhov, 2022).* The embryonic pole contains the inner cell mass (ICM) anchored by overlying polar trophectoderm (TE) cells, whereas the abembryonic pole consists of mural TE cells bounding the blastocoel. The increasing size of blastocoel induces blastocyst expansion until the resulting force on TE mural cells rises to a level that triggered cell-cell junction disruption *(Chan et al, 2019).* This event facilitates hatching and occurs when embryo has reached the uterus and is ready for the implantation in endometrium (occurring at approximately 4 days post fertilization in mice).

1.5 Molecular regulation of first lineage determination

The cellular changes that define initial polarization, and subsequently cell fate determination later, are governed by a tightly regulated molecular network. One of the earliest and most abundant marker differentially distributed between polar and apolar cells is YAP protein *(Nishioka et al, 2009)*. YAP activity can be regulated by ligand-dependent pathway, metabolic signals, and mechanotransduction, but its primary regulator is Hippo signalling pathway *(Totaro et al, 2018).* In mammals, this core cascade comprises the MST1/2 and Lats1/2 kinases, which phosphorylate YAP to inhibit its nuclear

translocation *(Zhao et al, 2007)*. Conversely, when YAP remains unphosphorylated, it translocates into the nucleus, where it functions as transcriptional factor *(Pfeffer et al, 2024)*.

During early embryonic stages, from the 4-cell to the early 8-cell stage, prior to the onset of compaction, YAP assumes a nuclear localization in all blastomeres *(Nishioka et al, 2009)* through a process mediated by its cofactor Tead4 *(Zhu et al, 2020)*. From 9-16 cells, cell polarization restricts YAP presence exclusively to polarized cells *(Korotkevich et al, 2017)*. This spatially change in YAP localisation is given by different pathways set in apolar and polar cells. In inner and apolar cells, adherent junction, composed by E-Cad and α- and β-catenin, allows NF2 binding in basolaterally position and the following recruitment of AMOT to the same basolateral domain. AMOT is phosphorylated at Serine-176; this modification allows AMOT to assemble into a complex with Lat1/2, thereby activating Hippo signalling and directing YAP to degradation *(Hirate et al, 2013)*. In contrast, in polar cells, AMOT is sequestered by the apical actomyosin ring. Specifically, RhoA prevents AMOT phosphorylation, enabling AMOT to bind F-actin. Consequently, Lats1/2 is not activated and Hippo signalling pathway remains silenced. YAP can enter the nucleus where it promotes TE marker CDX2 transcription *(Strumpf et al, 2005; Ralston et al, 2008)* and inhibits SOX2 and OCT4 expression *(Wicklow et al, 2014)*. By the 32-cell stage, a positive feedback loop is established between polar maintenance and YAP activity *(Frum et al, 2018).* By blastocyst stage, cell fate specification is determined, defining TE lineage marked by CDX2 and ICM by OCT4. Although both transcription factors are expressed at earlier embryo developmental stages their expression becomes mutually exclusive and strictly restricted to their respective cell lineages only at this phase *(Dietrich and Hiiragi, 2007).* Both CDX2 and OCT4 represent essential lineage-specifying factors for embryo viability *(Nichols et al, 1998; Strumpf et al, 2005).* As shown in Figure 1.5.1*,* the separation between OCT4 and CDX2 in, respectively, ICM and TE, is maintained by the mutual repression, reinforced by lineage-specific gene regulatory networks *(Sasaki et al, 2007).* In TE pathway*, Eomes*, a transcriptional factor among T-box family, is required for trophoblast development; indeed, *Eomes* knockout embryos fail to develop post-implantation *in vitro (Russ et al. 2000).* Downstream to CDX2 and Eomes, Ets-transcription factor (Elf5) reinforces the expression of both upstream factors *(Ng et al, 2008)*, establishing a positive feedback regulation that guarantees TE lineage maintenance. In embryonic stem cells (ESCs), when Elf5 is suppressed by DNA methylation, cells differentiate in TE (Ng et al, 2008).

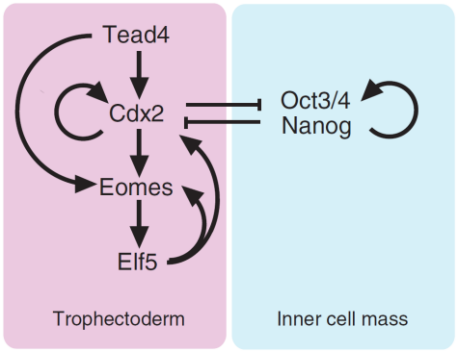

Figure 1.5.1 *Transcriptional network involved in cell lineage determination and maintenance*

Regarding ICM, the lineage specification and pluripotency upkeep is ensured by OCT4 which acts as a master regulator. OCT4 is a transcription factor characterized by two DNA-binding domains joined by a flexible linker. This structure conformation allows OCT4 to interact with other factors *(Rizzino and Wuebben, 2016).* Within these, a prominent candidate is SOX2, also involved in pluripotency maintenance, which has the same binding site of the master regulator. OCT4 and SOX2 form a heterodimer and act synergically on their target genes *(Swain et al, 2020).* A well-characterized target of OCT4/SOX2 is NANOG, which encodes another pivotal transcriptional factor expressed only in ICM cells. NANOG is particularly relevant for epiblast formation, exerting its primary function in late blastocyst *(Mitsui et al, 2003)*. OCT4 dynamically regulates intracellular NANOG expression, maintaining low basal levels during early preimplantation development before upregulating its expression during the transition toward the late blastocyst stage *(Rizzino and Wuebben, 2016)*.

1.6 CYP effects on Murine Embryonic Stem Cells

Given the extraordinary complexity of the molecular signalling networks governing preimplantation development, many of which remain incompletely understood, this highly orchestrated process is particularly susceptible to disruption by xenobiotics and environmental chemical compounds. Subtle perturbations in cellular polarization, gene expression, or metabolic pathways during these early stages can have profound and lasting consequences on lineage specification and embryo viability. Despite this vulnerability, the potential toxicological impact of pyrethroids on preimplantation embryonic development remains remarkably understudied. To date, the only study related to CYP toxicity in mammalian preimplantation embryo development is the work conduct by Rebuzzini et al. (2020) in Laboratory of Biology and Biotechnology of Reproduction (LBBR), University of Pavia. The authors evaluated the effects of LD50 concentration of 0.3 mM CYP on mouse R1-ESCs, as an *in vitro* model to predict pyrethroid toxicity on ICM *(Rebuzzini et al, 2020).* Following a 72-hour exposure, the study assessed multiple toxicological endpoints, including apoptosis rate, cell growth,

ROS production, gene expression alteration and activation of oxidative stress genes *(Rebuzzini et al, 2020)*.

Results demonstrate that CYP negatively impact on R1-ESCs growth rate, by inducing two distinct apoptotic waves at 12 and 24 hours post-treatment. At 24h, ROS production increases, causing a persistent oxidative stress response evidenced by the upregulation of redox-related genes (*Sod1*, *Sod2*, *Cat*, *Gpx1*) at 48 hours. The activation of detoxification response starts at 24h with the induction of phase I (*Nqo1*) or phase II (*Ugt1a6*, *Gsta1*) genes, followed by the overexpression of the phase I gene *Cyp1b1* at 72 hours.

Altogether, these results indicate that in response to the pyrethroid administration, R1-ESCs activate both detoxification and oxidative-stress responses but these endogenous defences are insufficient to compensate CYP-induced damages, resulting on a lower growth rate compared to controls.

Regarding pluripotency maintenance, CYP altered *Nanog* and *Oct4* gene expression. Furthermore, in subsequent embryoid body differentiation assays, CYP treatment disrupted the expression of lineage-specific germ layer markers, including *Fgf5* (primitive ectoderm), *Brachyury* (mesoderm), and *Foxa2* (endoderm) *(Rebuzzini et al, 2020)*.

1.7 Preliminary data on Preimplantation Mouse Development

Building upon the study by Rebuzzini et al. (2020), the LBBR determined the optimal CYP concentration for treating preimplantation embryos. Specifically, embryos generated via *in vitro* fertilisation (IVF) were exposed to a wide range of CYP concentrations starting from (300 μM (corresponding to the LD50 previously identified in R1-ESCs) down to 100 μM, 10 μM, 1 μM, 100 nM, 10 nM, 1nM, 0,1 nM CYP, to identify the lowest dose capable of significantly impairing embryo development rates. CYP was added to the culture medium at 3 hours post insemination and maintained throughout preimplantation development up to the blastocyst stage. Statistical significance for the decreased embryo development rate was calculated by comparing the rates of 2-cell, 4-cell, morula and blastocyst stage between treated and untreated (control) embryos. As shown in Figure 1.7.1, the results demonstrate that 1 nM represents the minimal CYP concentration required to induce a significant reduction in developmental rates across all monitored preimplantation stages.

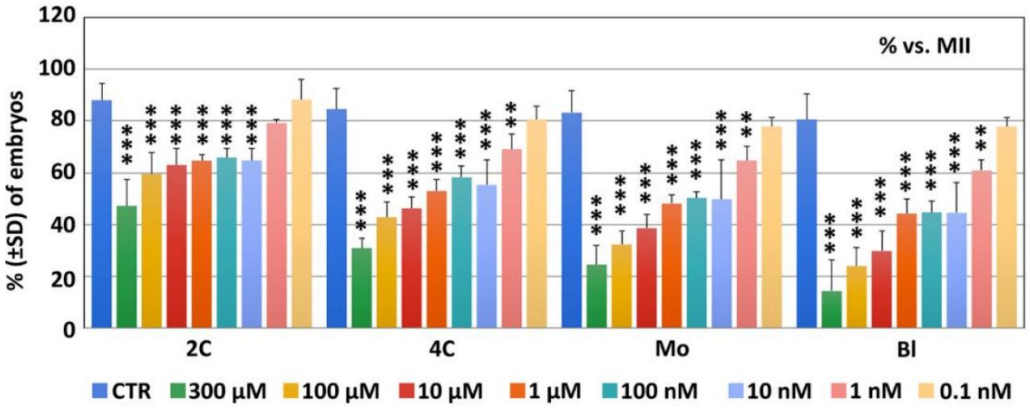

Figure 1.7.1 *Histogram of embryo percentages at different developmental stages cultured in the presence or in the absence of CYP. Asterisks correspond to statistical significance as follows: *p<0,05; **p<0,01; ***p<0,001*

2. AIM OF THE WORK

In the current literature, CYP is well known to negatively impacts various physiological system with its mechanisms of action and toxicological effects on reproductive function being extensively characterized in both male and female gonads. However, the potential impact of CYP during the critical window of preimplantation embryonic development remains largely unexplored. To address this gap knowledge, the primary aim of this Master's thesis was to investigate the developmental, morphological, and molecular effects of sub-lethal CYP exposure during mouse early embryogenesis in vitro.

To achieve this goal, mouse embryos were generated via *in vitro* fertilization (IVF) and, at 3 hours post-insemination (hpi), randomly allocated into two experimental conditions:

- Control group (CTR): Embryos cultured in standard M16 medium.
- Treated group (CYP): Embryos continuously exposed to 1 nM CYP in M16 medium up to the blastocyst stage.

The toxicological impact of CYP was systematically evaluated across three main biological levels:

- Developmental kinetics and yields: developmental yields of treated embryos, monitoring as preimplantation embryo development checkpoints for the comparison with CTR group 2-cells, 4-cells, morula and blastocyst;
- Morphological blastocyst quality: morphological CYP-treated blastocyst quality via quantitative immunofluorescence microscopy. DAPI staining was employed to quantify total blastomere numbers and identify pyknotic nuclei as an indicator of cell death. Simultaneously, immunolabeling for, OCT4 (marker for ICM) and CDX2 (marker for TE) was conducted to highlight cell distribution in lineage specification;
- Molecular profiling and pathway analysis: characterizing the transcriptional response of blastocysts using transcriptomic profiling combined with microarray technology combined to bioinformatic analyses, to identify the presence of differential expressed genes (DEGs) and deregulated pathways.

3. MATERIALS AND METHODS

3.1 Animals and reagents

Male and female mice of CD1 strain were used in this experimental setting. They were respectively 6 months and 4-8 weeks old and were bought from Charles River (Como, Italy). All procedures were performed in compliance with an experimental protocol (ministerial authorization No. 919/2023-PR) approved by the Animal Welfare Body (OPBA) of the University of Pavia and in accordance with European (2020/63/EU) and Italian (Dlvo 26/2014) regulations relating to the protection of animals used for scientific purposes approved by the Ministry of Health.

Mice were housed in a controlled environment with 60% humidity and a temperature of 22 °C of temperature. These parameters were kept stable under a 12:12 hours light/night cycle.

Animals were sacrified at the Interdepartmental Service Center Unified management of the Stabulation and Radiology activities of the University of Pavia; the procedure consisted of anaesthesia followed by cervical dislocation.

All reagents were purchased from Merck-Sigma unless otherwise specified.

3.2 In Vitro Fertilisation (IVF)

The procedure began with hormonal treatments in female mice to obtain a larger pool of competent oocyte for IVF. Specifically, the procedure started with an injection of 10 I.U mare serum gonadotropin (PMSG, Folligon, Intervet Srl Italy) to synchronize follicles maturation. After 48 hours, a second injection of 10 IU of human chorionic gonadotropin (hCG, Corulon, Intervet Srl) was administered to induce the superovulation 12-15 hours later.

At least 8 hours before the experiment, the media for the IVF procedure were prepared and equilibrated for at least 8 hours in a humidified incubator at 37°C with 5% CO_2 and 20% O_2 to reach a physiological pH 7.2. The chemical composition of each medium is showed in Table 3.2.1.

The first medium used was Whittingham (Wt) medium, characterized by 3% fetal bovine serum albumin (BSA). Its pH was adjusted to 8.0 by adding some drops of 0.5 M NaOH. The high glucose concentration makes it the ideal environment to carry out sperm capacitation and fertilization.

The second medium used is M2 supplemented with 0.4% of BSA. As with the Wt medium, the pH was corrected to 7.2 adding 0.5M NaOH. M2 medium was used during isolation of oocytes MII from the oviduct. To improve the oocyte's developmental competence, an M2-Ca2+free medium with 32.4 mM ETDA (M2-EDTA) was used as a pre-treatment *(Merico et al., 2020)*.

Finally, M16 medium was used for embryo culture. This medium contains a percentage of glucose that supporting the embryo pre-implantation development.

Table 3.2.1 *stock media's saline composition referred to 1L of medium. In M2-Ca2+free solution, CaCl2 *2H2O is not added in M2 stock medium*

WHITTINGHAM (Wt) STOCK MEDIUM (1L)		M16 STOCK MEDIUM (1L)		M2 STOCK MEDIUM (1L)	
NaCl	5.803 gr	**NaCl**	5.698 gr	**NaCl**	5.68 g/l
KCl	0.201 gr	**KCl**	0.356 gr	**KCl**	0.356 g/l
$NaHCO_3$	2.106 gr	**$CaCl_2 * 2H_2O$**	0.251 gr	**$CaCl_2 *2H_2O$**	0.251 g/l
$Na_2HPO_4 *12\ H_2O$	0.056 gr	**KH_2PO_4**	0.136 gr	**$MgSO_4 * 7H_2O$**	0.293 g/l
$MgCl_2 *6H_2O$	0.102 gr	**$MgSO_4$**	0.143 gr	**KH_2PO_4**	0.162 g/l
$CaCl_2 * 2H_2O$	0.264 gr	**Glucose**	0.036 gr	**$NaHCO_3$**	0.35 g/l
Glucose	1.000 gr	**$NaHCO_3$**	2.101 gr	**Phenol Red Na**	0.01 g/l
Sodium Pyruvate	0.055 gr	**EDTA (0.1mM)**	1.000 mL	**HEPES**	4.969 g/l
Sodiun Lactate (60%)	3.500 ml	**Sodiun Lactate (60%)**	5.530 ml	**Sodiun Lactate (60%)**	5.65 g/l
Phenol Red Na	0.010 gr	**Phenol Red Na**	0.010 gr		
Pen/Strep (50U/mL)	5mL	**Pen/Strep (50U/mL)**	5 mL	**Pen/Strep (50U/mL)**	5 mL
MilliQ Water	Up to 1L	**MilliQ Water**	Up to 1L	**MilliQ Water**	Up to 1L

The IVF began with the isolation of sperm from the cauda epididymis. The organ was punctured with a sterile 27 G needle and placed at the bottom of a tube, pre-heated to 37°C, containing 1500 ul of Wt medium. The vial was then incubated at 37°C in a humidified atmosphere of 5% CO_2 and 20% O_2 for 20 minutes. This step allowed for an initial selection of sperm based on motility, as only the most viable cells can swim up through the tube and reach the top of the tube (*Mahadevan and Baker, 1984*).

The sperm were collected by aspirating 400 µl from the upper layer of the supernatant. This aliquot constituted the capacitation drop, which covered with mineral oil and incubated for 40 minutes at 37°C in a humidified atmosphere with 5% CO_2 and 5% O_2 to allow the sperm to become competent for oocyte fertilization. The optimal sperm concentration for procedure was 1.8×10^6 sperm/ml. Sperm were counted by taking an aliquot from capacitation drop and using a Bürker counting chamber (as shown in Figure 3.2.1). Once the final number was determined, the sperm were diluted using fresh Wt medium. The following formula was used for count:

$$N.\ sperm/ml = M \times f.d. \times C$$

- *M* represents the average number of cells counted in ten randomly selected squares;

- *f.d.* is the dilution factor;
- *C* represents the volume constant, with depends on the chamber and the squares counted; in this case, C = 2.5×10^5 mL.

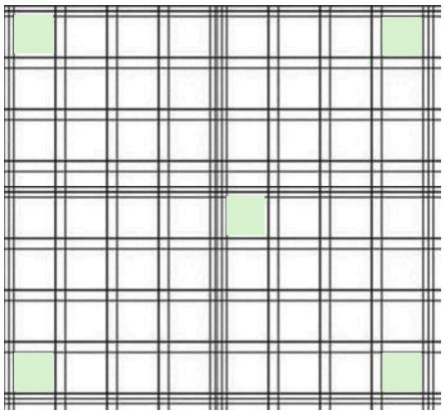

Figure 3.2.1 *Burker counting chamber with dials used for counts highlighted in green.*

Fifteen hours after hCG injection, the oviducts were isolated from the female mice and transferred into a Petri dish containing 500 µl of M2 medium. The organs were incised using a sterile 27G needle to allow the release and collection of cumulus–oocyte complexes (COCs) from the organ and their collection. Subsequently, the COCs were collected with a pipette and placed into a drop of M2-EDTA for 5 minutes. They were then washed twice in 400 µl drops of Wt medium to remove any residual of medium.
At this stage, both female and male gametes were ready for fertilization. They were transferred into a fertilization drop and incubated for 2 hours at 37°C in a humidified atmosphere of 5% CO_2 and 20% O_2 to allow fertilization to occur. Two hours later, the denuded oocytes were transferred into 50 µl drops of Wt medium and incubated for an additional hour in fresh Wt medium at 37°C and 5% CO_2. This step served a dual function: it removed excess sperm and allowed sperm those that have established contact with the egg cell to reach the perivitelline space and complete the fertilization process.

Oocyte showing the second polar body were considered successfully fertilized. These were washed in 20 µl drops of M16 medium to further remove residual sperms and Wt medium. Subsequently, they were transferred into drops of M16 medium (2 µl/embryo) for further development.

At this point, the presumptive zygotes were divided into two homogeneous experimental groups: treatment group (CYP) and control group (CTR). In the CYP group, embryos were cultured in M16 medium containing 1 nM CYP. The medium was prepared from a 600 mM CYP stock solution diluted in 100% dimethyl sulfoxide (DMSO), which was serially diluted to reach the final 1 nM CYP concentration. In CTR group, embryos were cultured in M16 medium containing 0.0015% DMSO, as concentrations equal to or below 0.1% have been shown to have no effect on embryonic development (*Merico et al, 2021*).

Embryo developmental rates were evaluated every 24 hours to monitor the 2-cell, 4-cell, morula, and blastocyst stages.

3.3 Double-immunofluorescence and image acquisition

Immunofluorescence was performed to evaluate the blastocyst quality. During the procedure, different dyes and markers were used to highlight specific cellular structures and characteristics. Three targets were analysed:

- OCT4: a marker for ICM (*Young, 2011*). It is a transcriptional factor and is considered a master regulator for the maintenance of pluripotency in embryonic stem cells *(Stirparo et al, 2021)*;

- CDX2: a transcriptional factor required for blastomeres differentiation into TE cells therefore acting as marker of this cell lineage *(Sritanaudomchai et al, 2009)*;

- Chromatin: labelled with the dye 4',6-diamidino-2-phenylindole (DAPI), which binds to A-T rich regions. To allow the identification of blastomeres nuclei and the counting of total cells within the blastocysts;

Blastocyst were fixed in 4% paraformaldehyde (PFA) diluted in 1X PBS for 30 minutes at room temperature (RT) and stored at 4 °C in 1X PBS supplemented with 0.01% Tween-20 until use. As a first step, blastocysts were permeabilized using 0.25% Triton X-100 solution in 1X PBS for 25 minutes at RT. To reduce non-specific binding, a blocking step was performed using a washing solution (WS, composition shown in Table 3.3.1) for 20 minutes at RT.

Table 3.3.1 *Wash solution composition*

WASH SOLUTION (10 ml)	
Salt phosphate buffer (1X PBS)	9,77 mL
Bovine fetal serum (FBS)	200 µL
Bovine serum albumin (BSA)	100 mg
Glycine	20 mg
Tween 20	20 µL

The embryos were incubated at 37 °C for 60 minutes with the primary anti-OCT4 antibody (catalog no. ab19857; Abcam), diluted 1:500 in 1X PBS. Excess antibody was washing 3 times for 15 minutes in WS at RT.

Subsequently, secondary anti-rabbit-488 antibody (catalog no. A11008; Molecular Probes), diluted 1:400 in WS, was then incubated with blastocysts at 37 °C for 45 minutes.

Regarding CDX2 staining, the procedure followed was identical to that described above, with the following differences: blastocysts were incubated overnight at 37 °C with the primary anti-CDX2 antibody (catalog no. 3977S; Cell Signaling) diluted 1:500 in 1XPBS. Excess of antibody was removed by washing 3 times for 15 minutes in WS at RT. Following this step, secondary anti-rabbit-555 (Molecular Probes), diluted in 1:400 in WS, was incubated with blastocysts at 37 °C for 45 minutes.

The nuclei were counterstained for 10 minutes with 0.25 µg/ml DAPI diluted in 1X PBS and mounted in drop of anti-fading medium containing 1,4-diazabicyclo[2.2.2]octane (DABCO). Immunodetection was performed using Leica SP8 confocal microscopy equipped with a white light laser. The fluorochromes (Alexa Fluor-488, Alexa Fluor-555 and DAPI) were excited at their proper wavelengths (respectively 488, 555 and 405 nm) using a 0.5 µm z-stack.

3.4 Blastomere's nuclei counting

Nuclei were counted in both CYP and CTR blastocysts using Fiji software (https://imagej.net/software/fiji/downloads). Specifically, nuclei were counted manually, distinguishing between viable or apoptotic nuclei. These two categories were differentiated based on morphological criteria: nuclei with fragmented shape or higher chromatin condensation are classified as apoptotic (*Kerr et al, 1972*) (Figure 3.4.1).

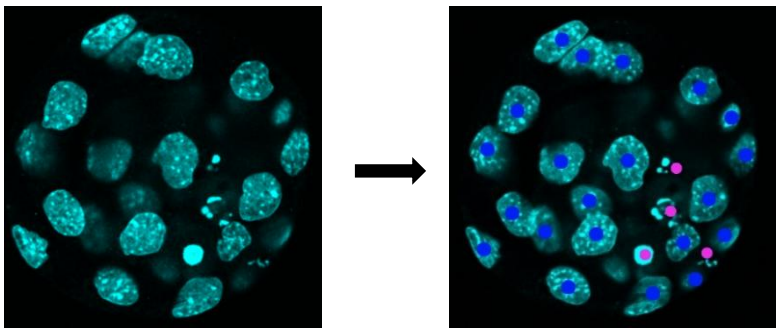

Figure 3.4.1 *example of blastomeres's nuclei couting: nuclei marked with blue are living nuclei while those marked in pink are considered apoptotic*

3.5 RNA extraction

Total RNA was extracted from both untreated and CYP-treated blastocysts using miRNeasy Micro Kit (Qiagen, Hilden, Germany) according to the manufacturer's instructions. All experiments were performed in triplicate.

Briefly, blastocysts were isolated and homogenized in QIAzol Lysis Reagent. Chloroform was added to the lysate, followed by incubation and centrifugation at 13,000 × g for 15 min at 4 °C to induce phase separation. The upper aqueous phase was transferred to a fresh tube, and the RNA was precipitated by adding ethanol. The sample was then loaded onto RNeasy MinElute spin column to allow total RNA binding to the membrane, followed by wash steps to remove potential contaminants. Finally, high-quality RNA was eluted in 14 µL in RNase-free water, quantified, and quality-checked using Tape Station system (Agilent, Santa Clara, CA, USA). Purified RNA samples were stored at -80 °C until further analysis.

3.6 Reverse Transcription and Quantitative Real-Time PCR (RT-qPCR)

Reverse transcription was performed in a final reaction volume of 20 µL containing 4 µL of total RNA, 1× PCR buffer, 5 mM $MgCl_2$, 4 mM of each dNTP, 0.625 µM oligo $d(T)_{16}$, 1.875 µM random hexamers, 20 U RNase inhibitor, and 50 U MuLV reverse transcriptase (all reagents from Thermo Fisher Scientific, Waltham, MA, USA). The thermal profile for cDNA synthesis comprised an initial step at 25 °C for 10 min, followed by reverse transcription at 42 °C for 15 min, and a final enzyme inactivation step at 99 °C for 5 min.

qPCR was subsequently conducted in duplicate using a 4-µL aliquot of the resulting cDNA (corresponding to one-fifth of the total RT volume) in a final reaction volume of 20 µL. The reaction mixture contained 200 nM of each forward and reverse primer and 1× MESA GREEN qPCR MasterMix Plus for SYBR Assay No ROX (Eurogentec, Liège, Belgium). Amplification was performed on a Rotor-Gene 6000 real-time rotary analyzer (Corbett Life Science, Sydney, Australia) to evaluate the transcript levels of *Ezh2*, *Smad7*, *Trim59* and *Tet2*. The thermal cycling conditions consisted of an initial denaturation at 95 °C for 5 min, followed by 40 cycles of denaturation at 95 °C for 10 s, annealing at 60 °C for 15 s, and extension at 72 °C for 20 s.

Comparative quantification was performed using Rotor-Gene 6000 Series Software 1.7. Expression levels of the target genes were normalized to the endogenous reference gene *Beta-2 microglobulin* (*B2m*).

3.7 Transcriptome Microarray Analysis

Global transcriptomic profiling was performed using the Clariom™ S Mouse Array platform (Applied Biosystems, Thermo Fisher Scientific, Waltham, MA, USA). Microarray target preparation was carried out on blastocyst total RNA samples using the GeneChip™ WT Pico Reagent Kit

(Applied Biosystems, Thermo Fisher Scientific), following the manufacturer's low-input protocol starting from total RNA within the recommended range (500 pg–10 ng).

Briefly, total RNA was reverse-transcribed to generate first-strand cDNA, followed by second-strand synthesis. A synthetic adaptor sequence was then ligated to the 3' end of the resulting cDNA molecules. Adaptor-tagged cDNA was subsequently amplified via Whole Transcriptome Amplification (WTA) using a high-fidelity PCR master mix. The amplified single-stranded cDNA (ss-cDNA) product was purified using magnetic beads, fragmented, and terminal-labeled with biotin in accordance with the manufacturer's instructions.

Biotinylated cDNA targets were hybridized onto Clariom™ S Mouse Arrays using the GeneChip™ Hybridization, Wash, and Stain Kit. Hybridization was conducted in a GeneChip™ Hybridization Oven 645, while washing and staining steps were performed on a GeneChip™ Fluidics Station 450 (Applied Biosystems). Microarray chips were scanned using the GeneChip™ Scanner 3000 7G controlled by the Affymetrix™ GeneChip™ Command Console™ (AGCC) software (ver. 4.0, Thermo Fisher Scientific).

Raw scan image data (.CEL files) were processed and analyzed using Transcriptome Analysis Console (TAC) software (ver. 4.0.2, Applied Biosystems). Array data normalization and signal summarization were performed using the Signal Space Transformation Robust Multi-Chip Analysis (SST-RMA) algorithm. The Detected Above Background (DABG) cutoff was set at $p < 0.05$, and the Area Under the Curve (AUC) threshold for positive-versus-negative control signal distribution was set at ≥ 0.70. Differentially Expressed Genes (DEGs) were identified using a one-way between-subjects ANOVA, applying the following statistical thresholds: an unadjusted p-value < 0.05 combined with an absolute Fold Change $|\mathrm{FC}| \geq 1.5$ ($\mathrm{FC} \geq 1.5$ for upregulated transcripts and $\mathrm{FC} \leq -1.5$ for downregulated transcripts).

3.8 Bioinformatic and Pathway Analysis

Differentially Expressed Genes (DEGs) identified from the microarray dataset (absolute fold change $|\mathrm{FC}| \geq 1.5, p < 0.05$) were subjected to bioinformatic analysis using two complementary platforms: Ingenuity Pathway Analysis (IPA) and the STRING/Cytoscape workflow.

Core functional and toxicological analyses were performed using IPA (QIAGEN Digital Insights, Redwood City, CA, USA) to identify significantly enriched canonical pathways, biological functions, and disease/toxicological categories associated with the DEG dataset. Downstream effect analysis and molecular interaction networks were algorithmically generated; network selection prioritized

constructs with high direct DEG representation over those relying predominantly on predicted or indirectly connected nodes.

To investigate functional protein-protein interaction (PPI) networks, the STRING database (ver. 12.0, *Mus musculus* organism setting) was queried using the DEG list. The resulting PPI network was imported, clustered, and visualized using Cytoscape software (ver. 3.10.0). Functional enrichment analysis within STRING was conducted across Gene Ontology (GO) categories (Biological Process, Molecular Function, and Cellular Component) as well as KEGG, Reactome, and Monarch pathway databases. Terms and pathways exhibiting a Benjamini-Hochberg False Discovery Rate (FDR) adjusted p-value < 0.05 were considered statistically significant.

3.9 Functional Annotation and Literature-Based Gene Screening

To investigate the potential molecular mechanisms and biological pathways disrupted by cypermethrin (CYP) exposure, the identified Differentially Expressed Genes (DEGs) were subjected to a structured literature-based screening using the National Center for Biotechnology Information (NCBI) PubMed database.

Each DEG was systematically cross-referenced against published peer-reviewed literature to evaluate its functional relevance within the context of preimplantation embryo development. Search queries combined individual gene symbols with a curated panel of 18 developmental keywords, categorized as follows:

- Preimplantation Morphogenesis and Events: *preimplantation*, *morula*, *blastocyst*, *blastulation*, *blastocoel*, *hatching*, *implantation*, *embryo segmentation*, and *gastrulation*;
- Lineage Specification and Germ Layers: *trophectoderm*, *inner cell mass*, *epiblast*, *hypoblast*, *endoderm*, *ectoderm*, and *mesoderm*;
- Transcriptional Transitions**:** *embryonic genome activation* and *zygotic genome activation*.

Genes with documented roles in any of these developmental processes were further prioritized for functional enrichment analysis and downstream pathway interpretation.

3.10 Statistical Analysis

All statistical analyses were performed using GraphPad Prism software (version 10.4.2, GraphPad Software, Boston, MA, USA). Prior to statistical testing, data normality and homoscedasticity were

evaluated. Quantitative differences between two experimental groups (CTR vs. CYP) were analyzed using an unpaired, two-tailed Student's *t*-test; percentage and proportional data (e.g., percentage of dead cells, ICM/TE cell proportions) were subjected to arcsine square-root transformation prior to parametric testing when necessary.

Data are expressed as the mean $\pm$ standard error of the mean (SEM). The exact number of analyzed blastocysts (n) and independent experimental replicates are indicated in the respective figure legends. Statistical significance was defined as $p < 0.05$, with significance levels denoted as follows: $* p < 0.05$,$p < 0.01$, $*** p < 0.001$, $**** p < 0.0001$, and ns = not significant.

4. RESULTS AND DISCUSSION

4.1 CYP disrupts preimplantation embryo development

At two hours post insemination (h.p.i), embryos derived from IVF were randomly allocated in two experimental groups, homogeneous in quality and number of embryos.

- Control group **(CTR)**: Embryos cultured in M16 medium supplemented with 0.0015% v/v dimethyl sulfoxide (DMSO).
- Treated group **(CYP):** Embryos cultured in M16 medium containing 1 nM CYP.

To systematically track developmental kinetics and yields, morphological checkpoints were evaluated at 24-hour intervals matching the parameters established in preliminary trials: 2-cells (24 h.p.i), 4-cells (48 h.p.i), morula (72 h.p.i) and blastocyst (96 h.p.i). This standardized temporal framework ensured precise comparability between historical controls, preliminary data, and final experimental outcomes.

The developmental rates for both cohorts are summarized in Table 4.1.1. Continuous exposure to 1 nM significantly reduces significantly embryo development yield ($p<0.05$) starting from 4-cell stage through blastocyst stage. At 96 hpi, blastocyst conversion rates in the CYP group exhibited an approximate 40% reduction compared to the control group. This massive decrease trend was confirmed was further confirmed when calculating efficiency relative to the 2-cell stage (100%), which revealed an overall 25% absolute drop in blastocyst formation in treated embryos. These findings align with preliminary observations, confirming that early nanomolar exposure to CYP compromises cleavage progression and blastocyst rate.

Table 4.1.1 *Embryonic developmental rates of CTR and CYP group. Data were obtained from three independent experiment (N=3) and are reported as %* ± DS. *Rates showed in italics were calculated considering 2-cell as 100%. The total number of embryos analysed is shown in parentheses. Asterisks indicate a statistically significant difference.*

Treatment	Replica	Preimplantation embryos developmental stage				
		MII	2-cell	4-cell	Morula	Blastocyst
CTR	3	100 (90)	94.2 ± 6.9 (85)	91.7 ± 10.0 (84)	90.5 ± 8.9 (83)	87.7 ± 9.7 93.0 ± 4.9 (80)
1 nM CYP	3	100 (160)	80.2 ± 2.4 (129)	70.6 ± 5.0* (114)	66.5 ± 4.7* (108)	61.5 ± 2.7* 76.6 ± 3.4* (99)

4.2 CYP negatively impacts on blastocysts quality

To evaluate whether CYP-induced developmental delay was accompanied by structural and cellular alterations, embryos reaching blastocyst stage, were fixed with 4% PFA and evaluated from a qualitative aspect using immunofluorescence technique. Blastocyst quality was evaluated using established morphometric criteria *(Pisko et al, 2021):*

- Total Blastomere Number (*N*): Quantified via DAPI nuclear counterstaining.
- Nuclear Pyknosis: Identified through DAPI-stained condensed or fragmented nuclear chromatin to calculate the total number and percentage of non-viable/dead cells.
- Lineage Allocation: Specifically determined using anti-OCT4 immunolabeling (marking the ICM) and anti-CDX2 immunolabeling (marking the TE).

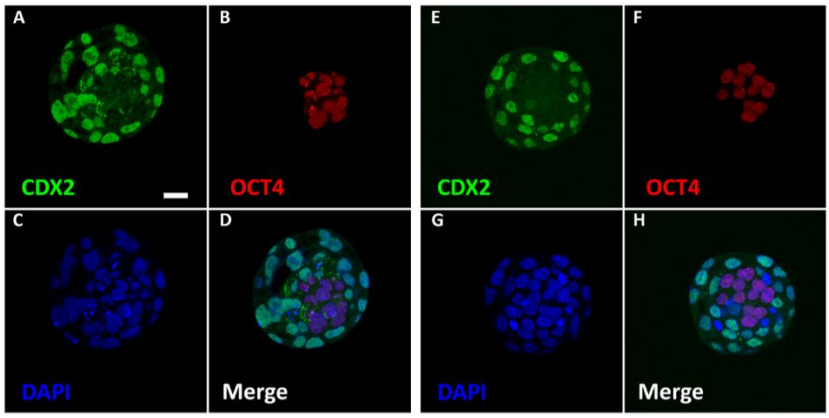

Figure 4.2.1 *Representative immunofluorescence images showing CDX2 positive (green) and OCT4 positive (red) blastomeres in control (CTR, A-D) and CYP treated (E-H) blastocysts, with nuclei counterstained by DAPI (blue). Scale bar used is 10µm.*

All statistical parameters were calculated using GraphPad Prism (version 10.4.2). All data collected are showed in Table 4.2.1 and are presented as mean ± standard error of the mean (SEM) to reflect precision.

Table 4.2.1 *Blastocyst quality assessment based on cell lineage and apoptosis analysis. Total cell number (DAPI-positive nuclei) along with the counts (%) of inner cell mass (ICM; OCT4-positive) and trophectoderm (TE; CDX2-positive) cells in blastocysts following treatment without (CTR) or with 1 nM CYP. Apoptotic cells (pyknotic nuclei) are reported as total DAPI-positive pyknotic counts and further categorized into ICM and TE lineages. Data are presented as mean ± SEM. p-values reflect statistical comparisons between CTR and treated groups, with statistically significant differences (p < 0.05) highlighted in bold.*

Marker		**Treatment Number ± SEM (%± SEM)**		
		CTR	1 nM	p value
Live	DAPI	53.8 ± 1.9	47.3 ± 1.9	**0.0159**
	OCT4-positive	18.5 ± 0.9 (29.8 ± 1.3%)	14.3 ± 0.9 (30.1 ± 1.4%)	**0.0021** (0.8858)
	CDX2-positive	43.9 ± 2.0 (70.2 ± 1.3%)	34.2 ± 2.4 (69.9 ± 1.4%)	**0.0043** (0.8858)
Dead	DAPI	2.5 ± 0.2 (5.8 ± 0.4%)	4.4 ± 0.3 (12.9 ± 1.1%)	**< 0.0001 (< 0.0001)**
	OCT4-positive	1.1 ± 0.2 (5.8 ± 0.9%)	1.6 ± 0.2 (12.2 ± 1.8%)	**0.0413 (0.0036)**
	CDX2-positive	2.3 ± 0.4 (5.7 ± 1.2%)	3.5 ± 0.4 (11.3 ± 1.6%)	**0.0352 (0.008)**

First, CTR group (n= 51) were composed of an average total of 53.8 ± 1.9 cells. Among these, 50.6 ± 1.8 blastomeres, displayed intact, healthy nuclear morphology.

Statistical comparison between total and viable cell numbers in the CTR group revealed no significant difference (Figure 4.2.2A). Furthermore, quantifying the baseline cell death rate showed a low, symmetrical distribution between the ICM (5.8±0.9%) and TE (5.7±1.2%) lineages (Figure 4.2.2B). This low background level of cell death reflects physiological programmed cell death, a process driven primarily by apoptosis during normal mammalian blastocyst development *(Brison, 2000)*.

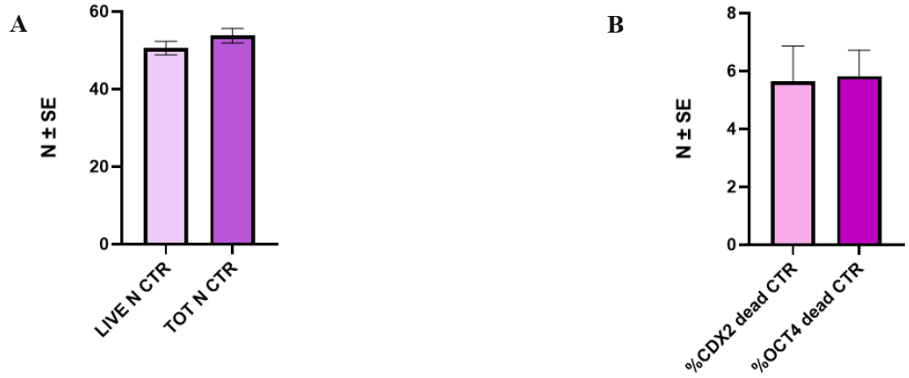

Figure 4.2.2 *Representative histograms showing:* ***A)*** *number of blastomeres with living nuclei morphology (50.6±1.8 cells) compared to total number of blastomeres composing blastocyst (53.8±1.9 cells) in CTR group;* ***B)*** *percentage of death rate in TE (5.7±1.2%) cross referenced with percentage of death rate in ICM (5.8±0.9%) in CTR group.*

During early embryogenesis, tightly regulated apoptosis eliminates damaged or developmentally compromised cells without compromising overall structural integrity. A critical threshold of viable blastomeres is essential to support subsequent morphogenetic events, such as uterine implantation and gastrulation.

Moreover, balanced cell death distribution between the ICM and TE maintains early cell fate specification. Excessive cell loss localized to the ICM would impair epiblast formation, destabilizing pluripotency networks through altered TE-derived inhibitory signalling *(Smith, 2005)*. Conversely, preferential apoptosis within the TE would weaken blastocyst adhesion and endometrial invasion, predisposing the embryo to early implantation failure or spontaneous abortion *(Guzman et al., 2019)*. Morphological comparison revealed a marked reduction in overall size in CYP-treated blastocysts compared to CTR (47.3±1.9 cells; p=0,0159). This phenotypic alteration correlated directly with a significant decrease in total blastomere count (Figure 4.2.3).

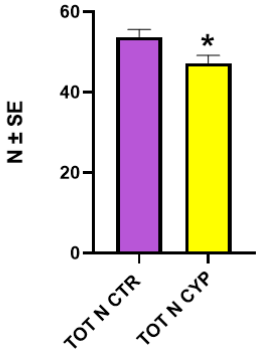

Figure 4.2.3 *Representative histogram showing cross-referencing between the total number of blastomeres in control group (purple) and treated group (yellow). The values obtained through statistical analysis are respectively 53.9*±1.9 and 47.3±1.9 cells. Asterisk indicates p value > 0.05

Mechanistically, a possible data interpretation is that CYP negatively impacts on physiological cellular mechanisms, disrupting the blastocyst expansion. During this phase, the number of blastomeres composing embryo increases and with it the blastocoel size. Prior to expansion, a physiological wave of PCD clears non-viable cells via phagocytic mechanisms *(Qu et al, 2007)*.
However, exposure to 1 nM CYP appears to disrupt this physiological balance by inducing excessive cellular damage. When the burden of apoptotic and pyknotic cells exceeds the embryonic clearance capacity, the remaining pool of viable blastomeres becomes insufficient to maintain morphogenetic progression. This dual insult, elevated cell death coupled with reduced functional cell mass, causes developmental arrest or collapse in a significant fraction of embryos. Consequently, the CYP-treated group contained a higher proportion of smaller, morphologically delayed early blastocysts, explaining the significant reduction in mean total blastomere count relative to CTR.
To verify the link between CYP exposure and cell death, as first step we have compared the number of living cells to the total number of cells composing CYP blastocysts. A significant (p=0,0359) difference has been observed (Figure 4.2.4A). It means that, contrary to what observed in CTR group, the number of living blastomeres composing CYP blastocysts is lower (41.6±1.9 cells) that the total number of cells (47.3±1.9 cells). At the same time, by a second analysis showed in Figure 4.2.4B, it came out that cell death rate in CYP-treated blastocyst is significantly higher ($p < 0,0001$) than in CTR (5.8±0.4%). These two results support our initial hypothesis: CYP treatment impacts on cell viability decreasing the number of living blastomeres and increasing cell death rate.

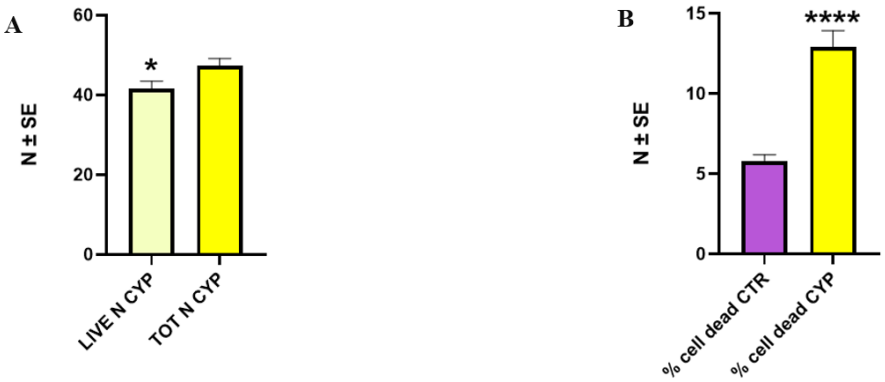

Figure 4.2.4 *Representative histograms showing:* ***A)*** *internal comparison in CYP group between number of cells with living nuclei morphology (41.6±1.9 cells) and total number of blastomeres composing blastocyst (47.3±1.9 cells);* ***B)*** *cross-reference of the percentage of dead cell in CTR group (5.8±0.4%) and in CYP group (12.9±1.1%). The number of asterisks above the column, reflects the statistical significance referring one asterisk to $p<0.05$ and four asterisks to $p< 0.0001$.*
As for the previous and following analyses, control group is coloured with purple while treated group with yellow

To determine whether CYP preferentially targeted a specific cell population, death rates were analysed across individual lineages. Specifically, the aim of them was first to check the distribution of cell death inside the embryo, to verify if CYP action was more negative in one of the two types of cell types present in the blastocyst, and second to evaluate how significant was the difference in blastomeres viability of ICM and TE in CYP group compared to CTR. The relative distribution of cell death between the ICM and TE showed no significant difference (p=0,7338) within the CYP group (Figure 4.2.5A), suggesting that CYP exerts an indiscriminate cytotoxic effect across the entire blastocyst.

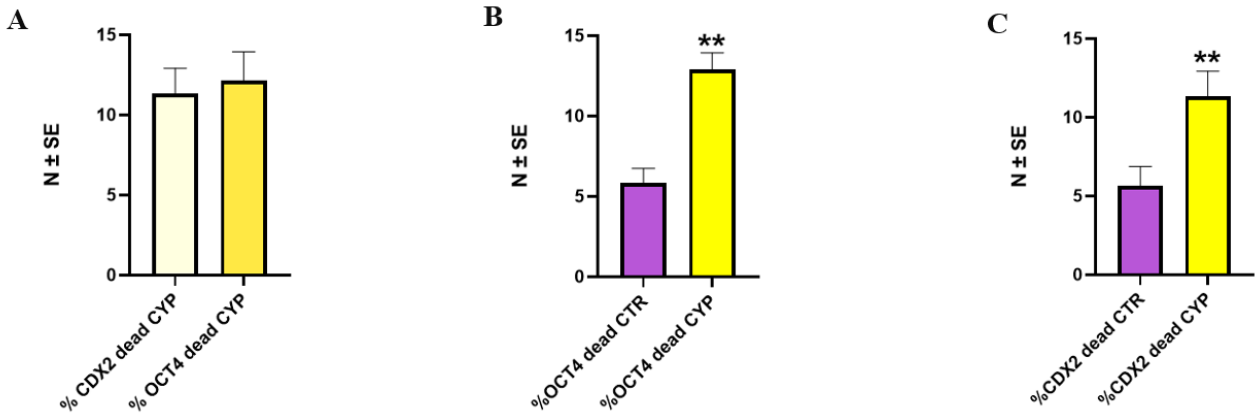

Figure 4.2.5 *Representative histograms showing:* ***A)*** *percentage of trophectoderm (so CDX2 positive) dead cells compared to ICM (OCT4 positive) dead cells. Values obtained from statistical analysis are respectively 11.3±1.6% and 12.2±1.8% and the lack of asterisks above the column indicate that no significant difference has been detected;* ***B)*** *comparison between the percentage of dead cell in ICM of control group and treated group one;* ***C)*** *cross-referencing between percentage of dead cell in TE of control group and treated group one.*
The two asterisks above the column in B and C refers to a p value < 0.01

However, direct comparison against control embryos confirmed that cell death rates were significantly elevated in both the ICM (Figure 4.2.5B) and the TE (Figure 4.2.5C).

Taken together, these analyses demonstrate that 1 nM CYP exposure severely compromises blastocyst quality through reduced embryonic size, decreased cell viability, and widespread induction of apoptosis across both inner and outer embryonic lineages.
To elucidate the molecular mechanisms and gene regulatory networks driving these cellular phenotypes, high-throughput transcriptomic profiling was subsequently performed.

4.3 Cypermethrin alters blastocyst transcriptome

The molecular effects of CYP were investigated through transcriptional analyses to characterize the gene expression profile of CYP-treated and CTR embryos. Three independent replicates were

analysed for each group, with each replicate comprising 50 blastocysts High-throughput microarray technology was used to evaluate transcriptomic profiles.

Bioinformatic analysis of 22,100 sequences revealed 508 DEGs in the CYP-treated group respect to CTR. Among these, 227 genes were upregulated (45%) and 221 downregulated (55%), displaying fold-change (FC) values ≥ 1.5 and ≤ 1.5 (Figure 4.3.1; Table 4.3.1). The expression of four genes (i.e. *Cdxl1, Ezh2, Tet2 and Trim59*) were validated by RT-qPCR (data not shown). These findings indicate that the transcriptomic profile of CYP blastocysts differs significantly from CTR embryos. Notably, this transcriptional alteration does not show a unidirectional trend (such as global repression or activation), but rather an almost equal distribution between up- and down-regulated genes.

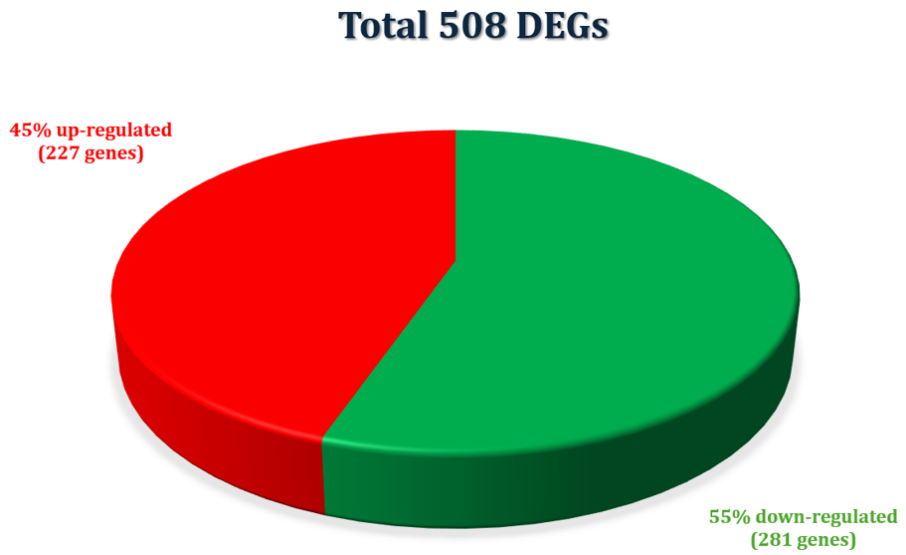

Figure 4.3.1 *Pie chart showing the distribution of the 508 DEGs identified in CYP-treated blastocysts compared to CTR. Downregulated genes are represented in green (281/508, 55%), while upregulated genes are represented in red (227/508, 45%).*

Table 4.3.1 Complete list of the 508 differentially expressed genes (DEGs) identified in 1 nM CYP-treated blastocysts. *Transcripts are categorized into upregulated and downregulated genes, alongside their corresponding fold-change (FC) values and statistical significance ($p < 0.05$, $|FC| \geq 1.5$).*

Up-regulated genes				Down-regulated genes					
Gene	**Fold-change**	**Gene**	**Fold-change**	**Gene**	**Fold-change**	**Gene**	**Fold-change**	**Gene**	**Fold-change**
Eno4	1,5	Fuca1	1,64	Rbm26	-3,14	Cnot1	-1,67	Desi2	-1,54
Mcph1	1,5	Gapt	1,64	Otud6b	-2,94	Hephl1	-1,67	Dip2b	-1,54
Slc22a8	1,5	Mctp1	1,64	Amz2	-2,91	Pacrg	-1,67	Eef1b2	-1,54
Slc44a3	1,5	Or11a4	1,64	Hdac9	-2,9	Slc25a26	-1,67	Fam21a	-1,54
Spsb2	1,5	Rnf122	1,64	Trim59	-2,7	Slc5a1	-1,67	Fgf13	-1,54
Ubr7	1,5	Clec4a1	1,65	Cab39	-2,57	Slc9c1	-1,67	Fundc1	-1,54
Abcd2	1,51	Rttn	1,65	Fsip1	-2,45	Lmx1a	-1,66	Gart	-1,54

Arfip2	1,51	Sox5	1,65	Haus2	-2,29	Myo9b	-1,66	Haus6	-1,54
Dact3	1,51	Ace2	1,66	Serpini2	-2,28	Or9q1	-1,66	Klb	-1,54
Dock8	1,51	Fam222b	1,66	Dmxl1	-2,25	Pcdh7	-1,66	Lrrtm1	-1,54
F5	1,51	Rfx4	1,66	Tmtc2	-2,24	Peak1	-1,66	Nab1	-1,54
Fbxo38	1,51	Tbx18	1,66	Tsnax	-2,23	Qrsl1	-1,66	Ncoa3	-1,54
Rfx3	1,51	Trabd	1,66	Ptpro	-2,18	Rnf2	-1,66	Slc25a31	-1,54
Sike1	1,51	Uap1	1,66	Smad7	-2,17	Tomm34	-1,66	Ttll11	-1,54
Usp21	1,51	Fstl5	1,67	Fastkd1	-2,15	Atg5	-1,65	Vps13c	-1,54
Vac14	1,51	Npnt	1,67	Sf3b1	-2,15	Elp4	-1,65	Vps26b	-1,54
Zcchc2	1,51	Smim15	1,67	Agl	-2,1	Lrch1	-1,65	Zc3h13	-1,54
Zfp512	1,51	Ascc1	1,68	Eif4g2	-2,1	Tia1	-1,65	Ddx18	-1,53
Asz1	1,52	Erp27	1,68	Adgre1	-2,09	Zfp821	-1,65	Dnajc1	-1,53
Ddx3x	1,52	Hsf1	1,68	Tbck	-2,09	Fam81b	-1,64	Hells	-1,53
Edar	1,52	Mvk	1,68	Fam124b	-2,08	Flvcr1	-1,64	Lamb3	-1,53
Fam243	1,52	Phospho1	1,69	Sparcl1	-2,05	Lypd5	-1,64	Msh3	-1,53
Fbxo36	1,52	Slc17a1	1,69	Rfc1	-2,04	Ndufaf4	-1,64	Rps27a	-1,53
Gldn	1,52	Fbxo8	1,7	Usp1	-2,04	Rrh	-1,64	Sf3a2	-1,53
Hpse2	1,52	Syvn1	1,7	Nptn	-2,03	Tmem87a	-1,64	Zbtb22	-1,53
Kif2b	1,52	Cep41	1,71	Fcho2	-2,02	Usp18	-1,64	Adcyap1r1	-1,52
Mb21d2	1,52	Gtf3c6	1,71	Gtf3c3	-2,02	Adgrl2	-1,63	Ap3m2	-1,52
Rhobtb1	1,52	Nynrin	1,71	Chsy3	-2	Apc	-1,63	Blmh	-1,52
Snx1	1,52	Vcam1	1,71	Fgf1	-1,98	Cntln	-1,63	Cep112	-1,52
Socs6	1,52	Bcorl1	1,72	C1galt1	-1,95	Csrnp2	-1,63	Ddx41	-1,52
Tceanc	1,52	Capn9	1,72	Canx	-1,95	Hnrnpm	-1,63	Dio2	-1,52
Yipf3	1,52	Wsb1	1,72	Ppp1r36	-1,95	Iws1	-1,63	Ggh	-1,52
Cdc16	1,53	Exosc7	1,73	Ctsc	-1,94	Lax1	-1,63	Gjb3	-1,52
Eefsec	1,53	Hpse	1,73	Tnks	-1,94	Mapk12	-1,63	Limd1	-1,52
Glyat	1,53	Zdhhc16	1,73	Pudp	-1,91	Ncoa4	-1,63	Lrriq1	-1,52
Hoxa2	1,53	Ccdc68	1,74	Rpl7l1	-1,91	Rrp36	-1,63	Nup188	-1,52
Krtap24-1	1,53	Cdh6	1,74	Usp24	-1,91	Sgk3	-1,63	Sbspon	-1,52
N4bp1	1,53	Exoc4	1,74	Ckap5	-1,9	Stam	-1,63	Sfi1	-1,52
Nell2	1,53	Fam193b	1,74	Fez2	-1,9	Tpm1	-1,63	Sntg1	-1,52
Nt5dc1	1,53	Kin	1,74	Nap1l2	-1,9	Acsl6	-1,62	Suz12	-1,52
Setd2	1,53	Ppp1r12b	1,74	Ap1s3	-1,89	Fbxw7	-1,62	Chst2	-1,51
Wars2	1,53	Scube2	1,74	Adgrd1	-1,88	Foxb1	-1,62	Cldn12	-1,51
Abcc9	1,54	Serpinb5	1,74	Clec9a	-1,88	Glp1r	-1,62	Hcn2	-1,51
Afap1l2	1,54	Acat1	1,75	Ctnna1	-1,88	Itgae	-1,62	Nfic	-1,51
Api5	1,54	Trim69	1,75	Unc5c	-1,88	Las1l	-1,62	Serpina9	-1,51
Atp13a4	1,54	Vapa	1,75	Ipo13	-1,87	Mal2	-1,62	Slc18b1	-1,51
Dcaf5	1,54	Dtl	1,76	Smurf1	-1,87	Mapk8ip1	-1,62	Tbc1d23	-1,51
Fam216a	1,54	Lonrf1	1,76	Zfp383	-1,87	Mipol1	-1,62	Tlcd2	-1,51
Hebp1	1,54	Lrrcc1	1,76	Rxfp2	-1,86	Prim2	-1,62	Tmem63c	-1,51
Mgat4c	1,54	Ado	1,77	Ddx59	-1,85	Slc25a19	-1,62	Aimp1	-1,5
Rgs1	1,54	Mib1	1,77	Dnal1	-1,83	Slc27a2	-1,62	Ift172	-1,5
Smpd2	1,54	Saysd1	1,77	Foxo1	-1,83	Spink7	-1,62	Plcb4	-1,5
Stkld1	1,54	Wasf2	1,77	Nps	-1,83	Tsen2	-1,62	Pms2	-1,5

Uqcc1	1,54	Xpo5	1,77	Slc38a11	-1,83	Aldh18a1	-1,61		
Acvr2b	1,55	Cc2d2a	1,78	Snapc1	-1,83	Cops2	-1,61		
Btnl9	1,55	Ei24	1,78	Twf1	-1,83	Map7	-1,61		
Cyb5r1	1,55	Rnaseh2a	1,78	Got2	-1,82	Smpdl3a	-1,61		
Dram2	1,55	Rnf167	1,78	Hdac2	-1,82	Taf1a	-1,61		
Hdac1	1,55	Pfdn4	1,79	Smc1a	-1,82	Uba2	-1,61		
Polr2c	1,55	Pnpla8	1,79	Fuom	-1,81	Zfp92	-1,61		
Psmb4	1,55	Zfp637	1,79	Sclt1	-1,81	Acaa2	-1,6		
Hadh	1,56	Ercc2	1,8	Fbxo43	-1,8	Disp1	-1,6		
L3mbtl4	1,56	Gxylt1	1,81	Mettl18	-1,8	Dlg1	-1,6		
Nox3	1,56	C9orf72	1,82	Pde1a	-1,8	Elmod3	-1,6		
Pdzd11	1,56	Rhoc	1,83	Zc3h15	-1,8	Nadk2	-1,6		
Arsj	1,57	Crtam	1,84	E2f8	-1,79	Plag1	-1,6		
Dnah5	1,57	Ly96	1,84	Pmp2	-1,79	Rnf144b	-1,6		
Gins3	1,57	Pibf1	1,84	Rgs9bp	-1,79	Slitrk6	-1,6		
Paics	1,57	Prpf18	1,84	Gimap7	-1,78	Ube2g2	-1,6		
Sit1	1,57	Slc25a44	1,84	Pi15	-1,78	Ubtfl1	-1,6		
Tlr1	1,57	Scn2a	1,85	Cacng2	-1,77	Ubxn2a	-1,6		
Vip	1,57	Cacna1a	1,86	Cmtr2	-1,77	Vsig1	-1,6		
Adgrl1	1,58	Ccdc93	1,86	Copa	-1,77	Arfip1	-1,59		
Ing2	1,58	Dgkk	1,87	Nfrkb	-1,77	G3bp2	-1,59		
Lipa	1,58	Ints7	1,87	Tmem171	-1,77	Pik3c2b	-1,59		
Mecom	1,58	Mlip	1,87	C8b	-1,76	Ppfibp1	-1,59		
Pitpnm2	1,58	Spata9	1,87	Mstn	-1,76	Rufy1	-1,59		
Ptgfrn	1,58	Kpna3	1,89	Ndel1	-1,76	Ssbp2	-1,59		
Rab5a	1,58	Il31ra	1,9	Asprv1	-1,75	Tarbp1	-1,59		
Rnf186	1,58	Mrc1	1,9	Dclre1a	-1,75	Tbc1d13	-1,59		
Ssna1	1,58	Rab39b	1,9	Mdga2	-1,75	Cyth4	-1,58		
Vat1	1,58	Crlf3	1,91	Sorbs1	-1,75	Htt	-1,58		
Amtn	1,59	Nox4	1,91	Xrcc5	-1,74	Mnd1	-1,58		
Clint1	1,59	Sesn1	1,91	Xrn2	-1,74	Myrfl	-1,58		
Gpr183	1,59	Tet2	1,91	Cnbd2	-1,73	Ppp1r12a	-1,58		
Rnf13	1,59	Wdr83	1,91	Pygb	-1,73	Supt3	-1,58		
Scfd1	1,59	Nfxl1	1,92	Rab12	-1,73	Svil	-1,58		
Scn1b	1,59	Sort1	1,94	Efcab7	-1,72	Vav3	-1,58		
Slc1a5	1,59	Anapc7	1,95	Rcbtb1	-1,72	Agbl1	-1,57		
Cenpv	1,6	Sulf2	1,95	Rrm2	-1,72	Chodl	-1,57		
Cyp26a1	1,6	Zmym5	1,97	Tmem168	-1,72	Fgfr2	-1,57		
Ebag9	1,6	Exo1	1,98	Zcchc7	-1,72	Mmp16	-1,57		
Ly86	1,6	Gtf3a	1,98	Arnt	-1,71	Por	-1,57		
Psmc3	1,6	Ezh2	2	Cdv3	-1,71	Arpp19	-1,56		
Slc1a1	1,6	Dap3	2,03	Efnb2	-1,71	Bcr	-1,56		
Adcy2	1,61	Lmln	2,05	Lgals12	-1,71	Fgfbp1	-1,56		
Bcl2l14	1,61	Arl4a	2,08	Swt1	-1,71	Gapvd1	-1,56		
Dbf4	1,61	Nmrk1	2,08	Celf2	-1,7	Lpar6	-1,56		
Hyal4	1,61	Slc8a2	2,08	Dazl	-1,7	Ndufa6	-1,56		

Musk	1,61	Cxcl1	2,09	Lrrd1	-1,7	Nudt6	-1,56		
Nek4	1,61	Slc25a35	2,09	Myo9a	-1,7	Rfesd	-1,56		
Pex5l	1,61	Gdap1	2,1	P4hb	-1,7	Scgb1a1	-1,56		
Ptprq	1,61	Rpa3	2,11	Rbbp4	-1,7	Slc33a1	-1,56		
Dffb	1,62	Galk2	2,12	Xkrx	-1,7	Tmem237	-1,56		
Igfbp3	1,62	Meioc	2,17	Agmo	-1,69	Ube2e3	-1,56		
Lipn	1,62	Mbd5	2,19	Cd5l	-1,69	Ddhd1	-1,55		
Rad9b	1,62	Ccdc152	2,21	Fam3d	-1,69	Gstz1	-1,55		
Ryr2	1,62	Uaca	2,22	Rpl7a	-1,69	Myo6	-1,55		
Zyg11a	1,62	Ncam2	2,33	Bend7	-1,68	Phf8	-1,55		
Eif2ak2	1,63	Rfx6	2,55	Dkk4	-1,68	Abcc1	-1,54		
Fkbp7	1,63	Krt19	2,66	Golga7	-1,68	Adam2	-1,54		
Paqr7	1,63	Syne2	3,1	Scel	-1,68	Adap2	-1,54		
Rhno1	1,63	Tubgcp3	3,32	Stag1	-1,68	Adgra3	-1,54		
Toe1	1,63			Acot13	-1,67	Chfr	-1,54		

4.3.2 Functional Annotation and IPA Network Analysis

To functionalize and contextualize the identified DEGs, transcripts were linked to biological processes using Ingenuity Pathway Analysis (IPA) Network Analysis. This tool identifies and visualizes interactions between genes and other molecules based on curated evidence in the IPA database, highlighting both direct and indirect molecular relationships. This approach allowed the identification of the primary biological activities impacted by CYP treatment (Figure 4.3.2).

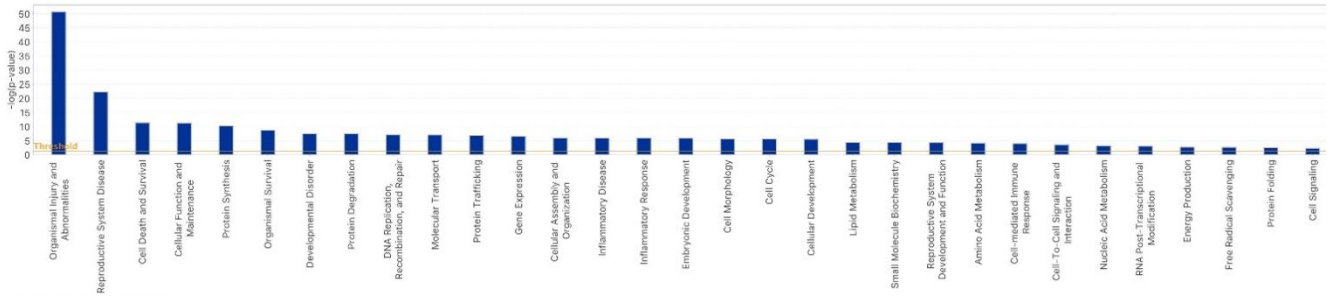

Figure 4.3.2 *Biological functions enriched in cypermethrin-treated blastocysts. Histograms showing biological processes involving the 508 DEGs in CYP exposed blastocysts compared to CTR. The statistical threshold level was set at p < 0,05.*

At the cellular level, the most altered processes, **(**Figure 4.3.3), involve mechanisms related to cellular homeostasis, maintenance of cellular function, and the regulation of cell death and survival. Gene expression was among the most heavily dysregulated processes:

- DNA replication, recombination, repair accounted for 71 matched transcripts;
- Protein synthesis accounting 242 of 508 DEGs;

- Protein degradation pathways were also significant altered, likely reflecting an adaptive response to increase protein turnover and clear misfolded or non-functional proteins resulting from insecticide-induced cellular damage.

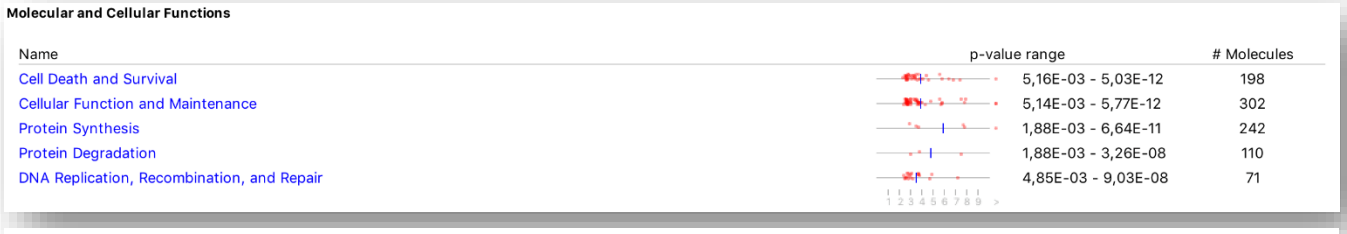

Molecular and Cellular Functions

Name	p-value range	# Molecules
Cell Death and Survival	5,16E-03 - 5,03E-12	198
Cellular Function and Maintenance	5,14E-03 - 5,77E-12	302
Protein Synthesis	1,88E-03 - 6,64E-11	242
Protein Degradation	1,88E-03 - 3,26E-08	110
DNA Replication, Recombination, and Repair	4,85E-03 - 9,03E-08	71

Figure 4.3.3 *tab representing the top 5 categories related to molecular and cellular functions with highest match and lowest p value to 508 DEGs of treated blastocysts*

To better understand the broader physiological effects of CYP on embryos, the five functional categories were analysed specifically for systemic physiology processes (Figure 4.3.4).

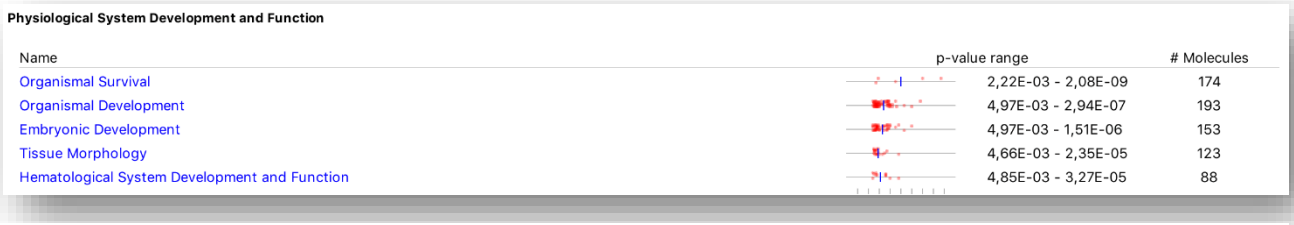

Physiological System Development and Function

Name	p-value range	# Molecules
Organismal Survival	2,22E-03 - 2,08E-09	174
Organismal Development	4,97E-03 - 2,94E-07	193
Embryonic Development	4,97E-03 - 1,51E-06	153
Tissue Morphology	4,66E-03 - 2,35E-05	123
Hematological System Development and Function	4,85E-03 - 3,27E-05	88

Figure 4.3.4 *tab representing the top 5 categories related to physiological system development and function with highest match and lowest p value to 508 DEGs of treated blastocysts*

Like the cellular analysis (Figure 4.3.2), CYP significantly impacts pathways involved in survival, as well as organismal and embryonic development. Notably, developmental dysregulation extended to later stages, as evidenced by alterations in transcripts associated with the development of the haematological system. Furthermore, 181 DEGs were linked to tissue morphology, highlighting structural alterations across embryonic tissues.

4.3.3 Toxicity Pathway Profiling (Top Tox Lists)

Following the identification of major cellular and systemic categories altered, the dataset mapped the "top tox list" (Figure 4.3.5), a curated collection of toxicity related categories and pathways linked to toxicological endpoints. IPA calculates for each tox category a p-value based on Fisher's exact test, indicating whether the dataset DEGs are significantly overrepresented in specific toxicological pathways. This analysis is therefore essential to relate DEGs to toxicological induced effects.

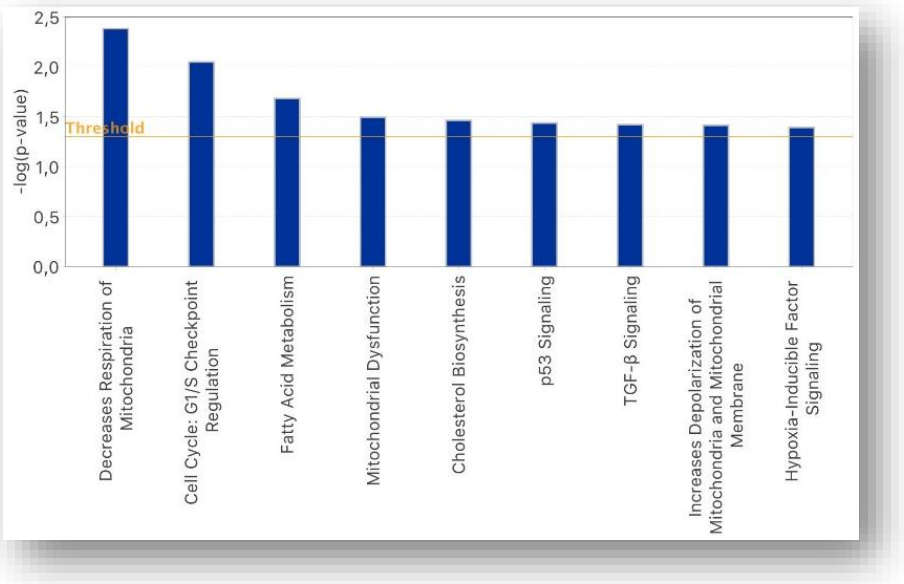

Figure 4.3.5 *Top toxicity categories enriched in cypermethrin-treated blastocysts. Histograms representing the main toxicological categories most significantly associated with the dataset DEGs, as identified by IPA*

The principal categories identified both metabolic and molecular alterations:

- Decreased respiration of mitochondria: this category showed the most significant match with DEGs and serve as a direct marker of cellular toxicity. Impaired mitochondrial function decreases ATP production, ultimately driving cells toward apoptosis *(Khan et al, 2022).* This molecular finding correlates directly with our morphological observations (Paragraph 4.2), where DAPI nuclear staining demonstrated a significantly higher cell death rate in CYP blastocysts.
- Cell cycle checkpoint alterations (G1/S Transition): dysregulation of the G1/S transition checkpoint regulation suggested direct or indirect genotoxic effects. CYP may induce massive DNA damages that fails the compensatory capacity of cellular repair machinery, leading to G1 cell cycle arrest. During preimplantation embryo development, cell cycle arrest prevents embryo cleavage and cell proliferation, preventing progression to subsequent developmental

stages and causing embryo degeneration. This mechanism aligns with the experimentally observed reduction in the percentage of embryos reaching key preimplantation stages *(Sfakianoudis et al, 2021)* (Table 4.1.1).

- Oxidative stress and lipid metabolism: enriched categories including, fatty acid metabolism, mitochondrial dysfunction and cholesterol biosynthesis represent core mechanisms altered by oxidative stress. Although CYP is known to induce oxidative stress in somatic tissues *(Clark and Symington, 2012; Elsawy et al, 2017)*, our findings demonstrate that this xenobiotic agent triggers comparable redox alterations in early embryonic stages.
- p53 and TGF-β signalling pathways: the significant enrichment of p53 and TGF-β signalling pathways highlights widespread cellular stress across blastomeres. Because these orchestrate essential cellular processes, including cell cycle control, apoptosis, and extracellular matrix remodelling, their disruption underscores broad toxicological damage *(Elston et al, 2012).*
- Mitochondrial membrane and Hipoxia-Induced Factor (HIF) signalling: the match of DEGs with these two sections highlights again the oxidative action of CYP on embryos. The insecticide treatment on blastomeres leads to ROS production, causing lipoperoxidation of membrane phospholipids and structural damage to mitochondrial respiratory chain complexes. The alteration of respiratory chain molecules causes the loss of proton gradient and subsequent membrane depolarization, amplifying ROS production and triggering HIF pathway activation *(Hagen et al, 2012)*.

Together, these results suggest that CYP impacts embryos systemically and disrupts core cellular processes.

4.3.4 Canonical Pathway Enrichment: Adipogenesis and RNA Polymerase III Assembly

To map DEGs onto well-characterized signalling networks, canonical pathway enrichment was performed using IPA (Figure 4.3.6)**.**

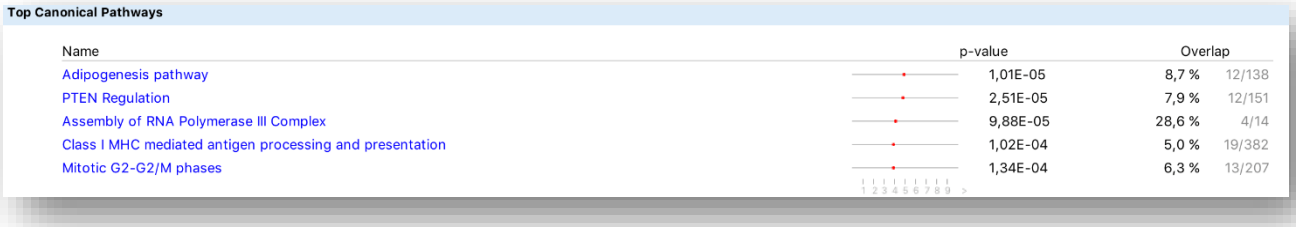

Figure 4.3.6 *Top canonical pathways enriched in cypermethrin-treated blastocysts. Summary of the principal canonical pathways exhibiting the highest gene overlap and statistically significant enrichment ($p < 0.05$) within the 508 DEGs, as identified by IPA*

Top Canonical Pathways identified by IPA included processes involved cell growth and proliferation regulation (PTEN signalling and G2-M mitotic phase control), transcriptional regulation (RNA polymerase III assembly complex); immune response (MHC class I antigen processing and presentation), and metabolism and cell differentiation regulation (adipogenesis pathway).

The adipogenesis pathway displayed the lowest p-value; thus, among all enriched pathways, it has the most statistically significant correspondence with the 508 DEGs analysed. It comprises a very complex signal cascade that guides the formation of mature adipocytes in differentiated tissues. In an embryonic context, however, the alteration of adipogenesis is considered a hallmark of metabolic and transcriptional reprogramming, causing the deregulation of energy production and cell differentiation *(Gaarenstroom et al, 2014).*

The key regulators of adipogenesis are the transcriptional factors PPARG and C/EBPα. They are modulated by extracellular molecules that bind surface receptors to activate an intracellular signalling cascade that either inhibit or enhance key regulators function *(Guo et al, 2024)*. The principal pathways implicated in this mechanism include TGF-β, WNT, BMP, GC, cAMP (Figure 4.3.7)

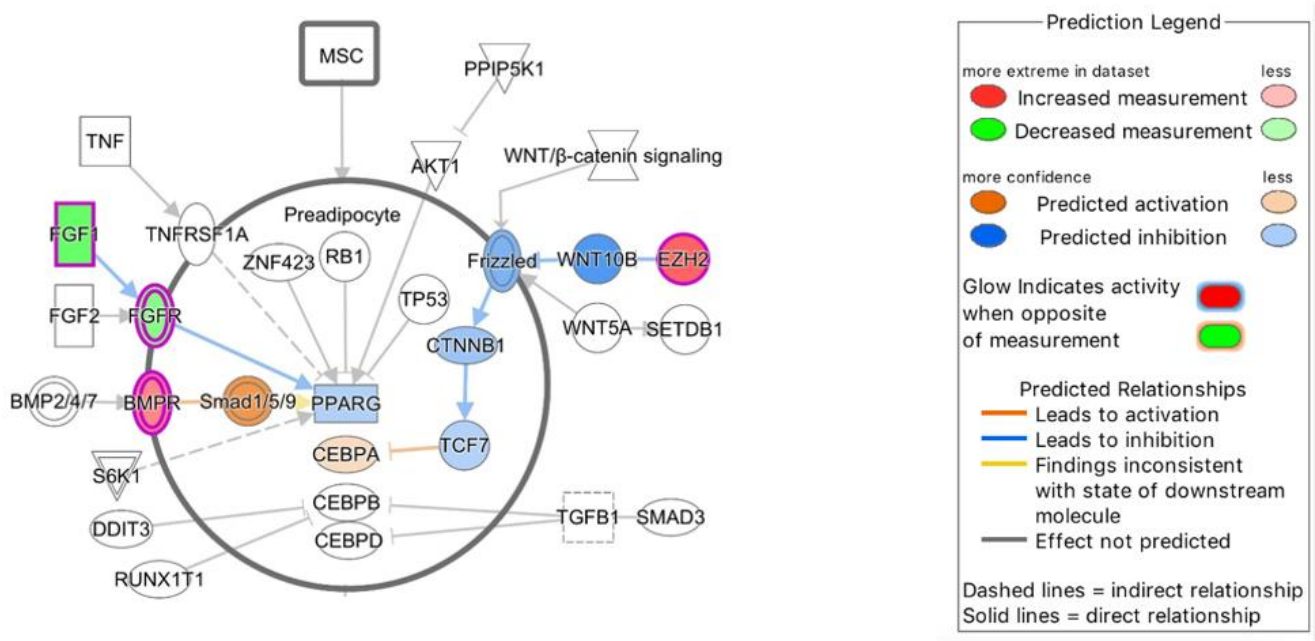

Figure 4.3.7 *Adipogenesis pathway including TGF-β, WNT, BMP, GC, cAMP signalling cascades*

The first pathway mentioned, is triggered the binding of TGF ligand to SMAD3, driving CEBPB and CEBPD inhibition that keeps the cell in an undifferentiated state. This negative regulation is reinforced by WNT signalling cascade, which is activated by the WNT ligand binding to the transmembrane receptor Frizzled, inducing CTNNB1 activation and accumulation. When CTNNB1 translocates into the nucleus, it associates to TCF7 mediating the direct inhibition of CEBPA transcriptional factor.

In this context, IPA highlighted a potential primary disruption of this mechanism: within the 508 DEGs, EZH2 upregulation is predicted to inactivate WNT10B, preventing its binding to Frizzled. EZH2 thus acts as an upstream inhibitor of WTN signalling cascade, ultimately weakening CEBPA inhibition. CEBP inactivation is essential to maintain cells in an undifferentiated state so an alteration of the WNT pathway could induce premature cell differentiation driven by metabolic reprogramming.
In contrast to TGF-β and WNT signalling cascade, BMP pathway promotes cell differentiation by acting on the PPARG transcriptional factor. The BMP ligand binds BMP receptor (BMPR) inducing the phosphorylation of Smad1/5/9. The activated complex associates with Smad4 and translocates into nucleus, where it promotes *Pparg* transcription. Once transcribed, translated and correctly folded, PPARG function as a transcription factor, activating genes involved in cell maturation and differentiation.
In CYP-treated blastocyst, this regulatory mechanism may also be altered because one of the key receptor proteins, BMPR, is upregulated in CYP group compared to CTR. Dysregulation of receptor expression could lead to enhanced activation of Smad1/5/9, amplifying the downstream signal *(Guo et al, 2024)*. Combined with the attenuation of downstream WNT signalling (resulting from the inhibitory activity of EZH2), the shift in cell fate toward maturation and differentiation would be substantially reinforced.
This global deregulation is further fuelled by FGF pathway alteration: among 508 DEGs, both FGF1 and its receptor FGF2R are downregulated (FC 1,98 and 1,57 respectively). This reduction in gene expression could impair the effectiveness of PPARG activation. Among all pathways involved in adipogenesis, the correlation between CYP treatment and FGF pathway alteration is particularly relevant, as this signalling cascade is fundamental for both metabolic regulation *(Zhang et al, 2018)* and embryonic development *(Krawczyk et al, 2022)*. Specifically, FGF1 is involved in glucose transport and uptake *(Zhang et al, 2018; Zhang and Yang, 2024)* and its abnormal expression is associated with metabolic disorders *(Zhang and Yang, 2024).* Regarding the role of the FGF1 and FGFR2 in embryonic development, Zhang et al (2018) demonstrated that *Fgfr2*−/− knockout mice display abnormalities in TE cell polarity and that decreased expression of FGFR2 leads to improper cell lineage specification. This occurs because reduced levels of FGF receptors prevent the transmission of intracellular signal, impacting on self-organisation of the embryo, likely through reduced cell proliferation *(Zhang et al, 2018).* Given that both FGF1 and FGFR2 are downregulated in CYP-treated blastocysts, similar deleterious effects likely occur in CYP group embryos.
Overall, the enrichment of adipogenesis pathway among demonstrates that multiple regulatory signalling cascades are altered in response to insecticide treatment, pointing to a major reorganization

of cellular metabolic and transcriptional programs and impair cellular energy status and differentiation processes.

Through IPA, it was also possible to highlight a potential correlation between CYP exposure and the deregulation of protein synthesis. As showed in Figure 4.3.6, the assembly RNA polymerase III complex pathway exhibited the highest overlap percentage (28,6%) since 4 out of 14 total genes involved in the cascade being differentially expressed in treated blastocysts.

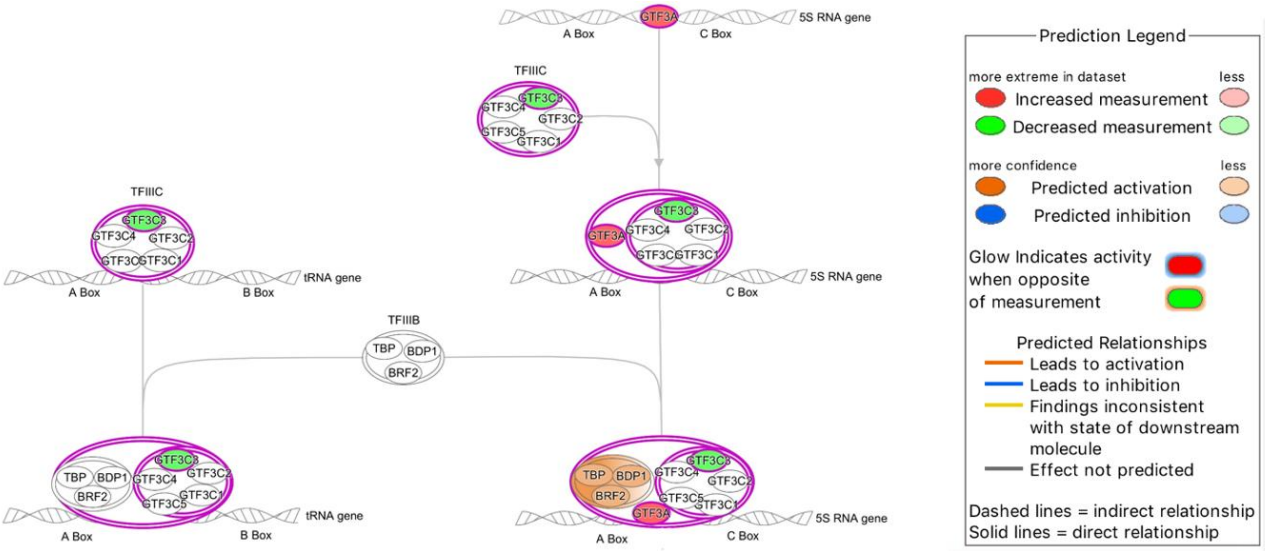

Figure 4.3.8 *Assembly of RNA polymerase III complex pathway*

As illustrated, the assembly of the RNA polymerase III complex can start via two different mechanisms depending on the promoter type. On the left part of Figure 4.3.8, initiation begins at a type II promoter, typically present in tRNA genes. This internal gene sequence is bounded by A and B boxes and is directly recognized by the transcription factor III C (TFIIIC). Upon binding the type II promoter, TFIIIC recruits TFIIIB to form the preinitiation complex (PIC) *(Kassavetis et al, 1990)*. RNA polymerase III then binds PIC and to initiate transcription.

On the right side of the figure, initiation occurs at a type I promoter of 5S rRNA gene. Here, PIC formation requires the prior binding to GTF3A protein to the internal control region (ICR) of 5S RNA gene *(Seifart et al, 1989).* In CYP group blastocysts, GTF3A is upregulated by 1.98 FC. This represents an alteration of physiological condition, as GTF3A overexpression typically occurs during early embryogenesis to improve ribosome assembly and therefore protein synthesis *(Diaz de Cerio et al, 2012; Valencia et al, 2017*), rather than at the end of preimplantation development.

GTF3A overexpression in treated blastocyst acts as a compensatory mechanism to replace ROS damaged proteins with newly synthetized and functional ones.

In both pathways represented in figure 4.3.8, GTF3C3 is coloured in green since it is downregulated (FC = 2.02). Physiologically in mice, GTF3C3 expression decreases progressively as blastomeres differentiate into specialized cell types *(Luzzani et al, 2011)*; thus, CYP may may negatively impact

pluripotency maintenance by inducing premature GTF3C3 downregulation. This downregulation might be partially compensated in 5S RNA pathway by the GTF3A upregulation, which aids TFIIB recruitment and activation. This analysis therefore underlines that RNA polymerase III assembly pathway is deregulated in CYP treated blastocyst due the altered expression of transcriptional complex proteins. because tRNA and 5S rRNA are essential for translation, modulating their expression may compromise protein synthesis efficacy and, consequently, diminishing the capacity of embryonic cells to sustain growth and proliferation during blastocyst development.

4.3.5 Identification of Specific Preimplantation Molecular Networks

Because IPA highlighted the potential disruption of fundamental biological processes following CYP treatment, we performed further analyses with to identify molecular networks specific to preimplantation embryo development. This approach aimed to clarify how CYP acts within this specific developmental window and address existing gaps in the literature.

To achieve this, the 508 DEGs were contextualized by searching PubMed for genes known to be involved in embryo development. Searches were performed using the gene symbol combined with the operator "AND" and specific keywords: segmentation, embryonic genome activation (EGA), morula, blastocyst, trophectoderm, inner cell mass, epiblast, hypoblast, hatching, gastrulation, ectoderm, mesoderm, endoderm. To exclude non-relevant results, exclusion filters were applied. The final search query was: "gene AND key word AND mammals NOT cancer NOT invertebrate NOT xenopus NOT Chinese hamster ovary cell NOT drosophila NOT chicken NOT fish".

This literature mining yielded 221 genes with at least one match among the selected keywords as showed in (Table 4.3.2). Among these, 88 DEGs were upregulated (40%) and 133 were downregulated (60%).

Table 4.3.2 *Out of 221 DEGs, the table shows those that are up- or down-regulated in the comparison between CYP-treated vs. CTR blastocysts. Gene symbols in bold and underlined font indicate a fold change* ≥ 2 *or* ≤ -2.

Keyword	N. (%) of DEGs	Genes	N. (%) of up-regulated genes	Up-regulated genes	N. (%) of down-regulated genes	Down-regulated genes
Segmentation	23 (10.4%)	*Acsl6, Agmo, Ckap5, Cntln, Dffb, Ebag9, Ercc2, Exo1, Gtf3a, Hoxa2, Map7, Pacrg, Rhobtb1, Rufy1, Sit1, Slc25a26, Slc25a31, Snapc1, Sox5,* ***Tubgcp3****, Vps26b, Xpo5, Zfp821*	11 (47.8%)	*Dffb, Ebag9, Ercc2, Exo1, Gtf3a, Hoxa2, Rhobtb1, Sit1, Sox5,* ***Tubgcp3****, Xpo5*	12 (52.2%)	*Acsl6, Agmo, Ckap5, Cntln, Map7, Pacrg, Rufy1, Slc25a26, Slc25a31, Snapc1, Vps26b, Zfp821*

EGA		24 (10.9%)	***Adgre1***, *Cdv3, Copa, Dtl,* ***Eif4g2***, *Elp4, Fbxo43, Hsf1, Iws1, Ndufa6, Pms2, Ppp1r36,* ***Ptpro***, ***Rbm26***, *Rfx3,* ***Rpa3***, *Rpl7l1, Scel, Sf3a2, Smc1a, Snx1, Svil, Tnks, Usp21*	6 (25.0%)	*Dtl, Hsf1,* ***Rpa3***, *Rfx3, Snx1, Usp21*	18 (75.0%)	***Adgre1***, *Cdv3, Copa,* ***Eif4g2***, *Elp4, Fbxo43, Iws1, Ndufa6, Pms2, Ppp1r36,* ***Ptpro***, ***Rbm26***, *Rpl7l1, Scel, Sf3a2, Smc1a, Svil, Tnks*
Morula		3 (1.4%)	*Ing2, Toe1, Wasf2*	3 (100.0%)	*Ing2, Toe1, Wasf2*	0 (0.0%)	-
Blastocyst	TE	**63 (28.5%)**	*Abcc1, Abcc9, Abcd2, Acat1, Acvr2b, Adam2, Apc, Arnt, Atg5, Btnl9, Canx, Cd5l, Cdh6, Cmtr2, Ctnna1a,* ***Cxcl1***, *Ddx3x, Dio2, E2f8, F5, Fbxw7, Fgf1, Fgf13, Fgfr2, Foxo1, Fundc1, Gjb3, Golga7, Hdac1, Hdac2,* ***Hdac9***, *Hebp1, Hephl1, Igfbp3, Itgae,* ***Krt19***, *Lamb3, Mcph1, Nab1, Ncoa3, Nynrin, P4hb, Pibf1, Rab39b, Rbbp4, Rhoc, Rnf2, Rrm2, Rxfp2, Ryr2, Serpinb5, Setd2,* ***Sf3b1***, *Slc1a5, Slc27a2, Slc5a1,* ***Smad7***, ***Sparcl1***, *Tbx18, Ubtfl1, Vcam1, Vip, Wdr83*	26 (41.3%)	*Acat1, Abcc9, Abcd2, Acvr2b, Btnl9, Cdh6,* ***Cxcl1***, *Ddx3x, F5, Hdac1, Hebp1, Igfbp3,* ***Krt19***, *Mcph1, Nynrin, Pibf1, Rab39b, Rhoc, Ryr2, Serpinb5, Setd2, Slc1a5, Tbx18, Vcam1, Vip, Wdr83*	37 (58.7%)	*Abcc1, Adam2, Apc, Arnt, Atg5, Canx, Cd5l, Cmtr2, Ctnna1a, Dio2, E2f8, Fbxw7, Fgf1, Fgf13, Fgfr2, Foxo1, Fundc1, Gjb3, Golga7, Hdac2,* ***Hdac9***, *Hephl1, Itgae, Lamb3, Nab1, Ncoa3, P4hb, Rbbp4, Rnf2, Rrm2, Rxfp2,* ***Sf3b1***, *Slc27a2, Slc5a1,* ***Smad7***, ***Sparcl1***, *Ubtfl1*
	ICM	**13 (5.9%)**	*Acaa2, Cenpv, Cnot1, Cops2, Dazl,* ***Ezh2***, *Mapk12, Ndel1, Suz12, Tet2,* ***Trim59***, *Ubxn2a, Zyg11a*	4 (30.8%)	*Cenpv,* ***Ezh2***, *Tet2, Zyg11a*	9 (69.2%)	*Acaa2, Cnot1, Cops2, Dazl, Mapk12, Ndel1, Suz12,* ***Trim59***, *Ubxn2a*
Epiblast		7 (3.2%)	*Adcyap1r1, Afap1l2, Asz1, Fez2, Hcn2, Hells, Mib1*	3 (42.9%)	*Afap1l2, Asz1, Mib1*	4 (57.1%)	*Adcyap1r1, Fez2, Hcn2, Hells*
Hypoblast		1 (0.5%)	*Dip2b*	0 (0.0%)	-	1 (100.0%)	*Dip2b*
Hatching		4 (1.8%)	*Myo6, Psmc3, Rps27a, Smpd2*	1 (25.0%)	*Smpd2*	3 (75.0%)	*Myo6, Psmc3, Rps27a*
Implantation		35 (15.8%)	*Adgra3, Aimp1, C1galt1,* ***Ccdc152***, *Chst2, Ctsc, Efcab7, Efnb2, Ggh, Hpse, Kif2b, Klb, Mapk8ip1, Msh3, Myo9a, N4bp1,* ***Ncam2***, *Nfrkb, Nox3, Por, Ppp1r12a, Psmb4, Pygb, Rab5a,* ***Rfc1***, *Scgb1a1, Slc25a19, Smpdl3a, Smurf1, Socs6, Sorbs1, Tpm1, Uba2, Usp18, Vav3*	9 (25.7%)	***Ccdc152***, *Hpse, Kif2b, N4bp1,* ***Ncam2***, *Nox3, Psmb4, Socs6, Rab5a*	26 (74.3%)	*Adgra3, Aimp1, C1galt1, Chst2, Ctsc, Efcab7, Efnb2, Ggh, Klb, Mapk8ip1, Msh3, Myo9a, Nfrkb, Por, Ppp1r12a, Pygb,* ***Rfc1***, *Scgb1a1, Slc25a19, Smpdl3a, Smurf1, Sorbs1, Tpm1, Uba2, Usp18, Vav3*
Gastrulation	Endoderm	9 (4.1%)	*Cyp26a1, Dkk4, Glp1r, Htt, Ipo13, Nox4, Scube2, Slc1a1, Xrcc5*	4 (44.4%)	*Cyp26a1, Nox4, Scube2, Slc1a1*	5 (55.6%)	*Dkk4, Glp1r, Htt, Ipo13, Xrcc5*
	Ectoderm	15 (6.8%)	*Ap3m2, Dock8, Edar, Foxb1, Ift172, Lpar6, Lrrtm1, Nap1l2, Rad9b, Sort1, Tlr1, Tmem237, Ubr7, Unc5c, Vac14*	7 (46.7%)	*Ap3m2, Foxb1, Ift172, Lpar6, Lrrtm1, Nap1l2, Tmem237, Unc5c*	8 (53.3%)	*Adcyap1r1, Apc, Atg5, Ckap5, Desi2, Dkk4, Dlg1, Fbxw7, Fgf1, Fgfr2, Foxb1, Foxo1, Gjb3, Glp1r, Hdac2, Hephl1, Htt, Ift172, Ipo13, Lpar6, Lrrtm1, Nap1l2, Phf8, Por, Ppp1r12a,*

							Scgb1a1, Smurf1, Suz12, Uba2, Unc5c, Xrcc5
	Mesoderm	24 (10.9%)	*Ace2, ArsJ, Cc2d2a, Cdc16, Cep41, Clec9a, Dact3, Desi2, Disp1, Dlg1, Exoc4, Fstl5, Mstn, Pcdh7, Phf8, Plag1, Slc22a8, Spink7, Sulf2,* ***Syne2****,* ***Tsnax****,* ***Uaca****,* ***Usp1****, Wsb1*	13 (54.2%)	*Ace2, Acvr2b, Cc2d2a, Cdc16, Ace2, ArsJ, Cc2d2a, Cdc16, Cep41, Dact3, Exoc4, Fstl5, Slc22a8, Spink7, Sulf2,* ***Syne2****,* ***Uaca***	11 (45.8%)	*Clec9a, Desi2, Disp1, Dlg1, Mstn, Pcdh7, Phf8, Plag1,* ***Tsnax****,* ***Usp1****, Wsb1*

Next, we mapped the molecular networks connecting these 221 DEGs to better characterize CYP action in embryos. Using STRING database, we generated an interaction network (Figure 4.3.9).

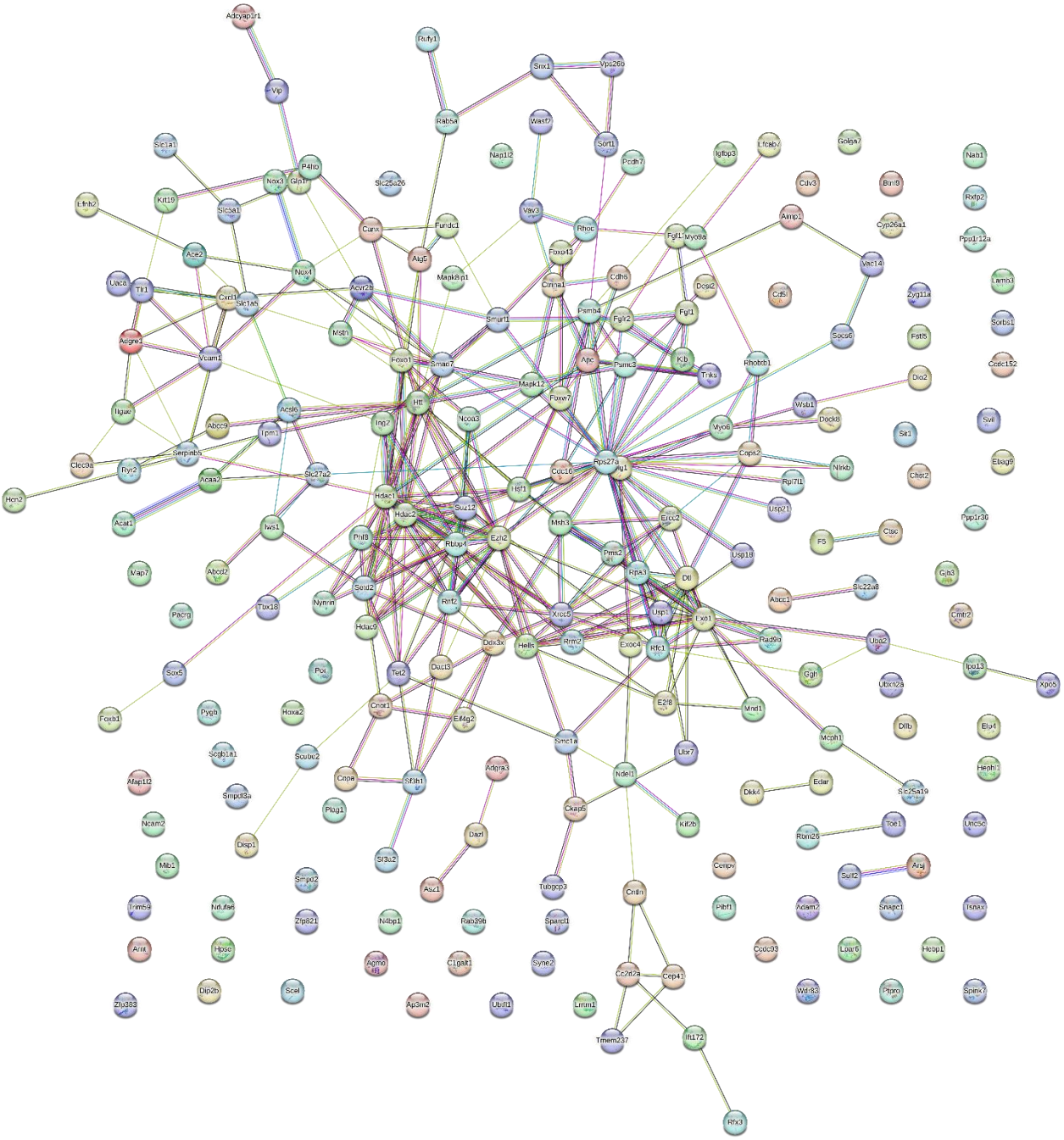

Figure 4.3.9 *String map on 221 DEGs with at least one match with one of the key words used in PubMed analysis*

Certain DEGs displayed higher connectivity than others, identifying them as key node regulators in the signalling cascades mediating the response to cypermethrin. To rank these central hub genes, we analyzed the network using CytoHubba plug-in of Cytoscape, setting “Degree” as parameter for the analysis. In the resulting network (Figure 4.3.10), nodes are coloured along a gradient from red to yellow based on connectivity: red nodes represent genes with the highest number of interactions, while yellow nodes denote lower connectivity.

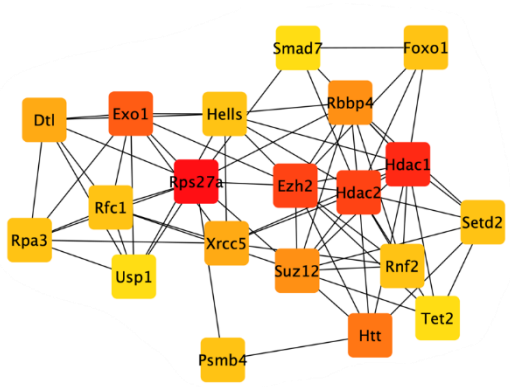

Figure 4.3.10 *Scheme representing top 20 ranking hub genes out of 221 DEGs with at least one match with one of the selected key words.*

As shown in Figure 4.3.10, the primary hubs identified were *Rps27a, Exo1, Ezh2, Hdac1* and *Hdac2*. RPS27A plays a dual action as ribosome component and small regulatory protein for ubiquitination, whereas EXO1 is involved in DNA mismatch repair and maintenance of genome stability *(Spies et al, 2015)*. EZH2, HDAC1 and HDAC2 represents fundamental components involved in transcription silencing via DNA methylation and histone deacetylation, respectively.

Given the importance of these master regulators of the cypermethrin response, we prioritized the functional analysis of EZH2, which was 2-fold upregulated in CYP blastocysts. Beyond its central network connectivity, literature evidence highlights its pivotal role in trophectoderm cell maintenance and differentiation, making it a key candidate to explain the observed developmental defects.

Ezh2 is the genic paralogue of *Ezh1* in embryonic cells. Together with EED, SUZ12 and histone-binding proteins Rbbp4 and/or Rbbp7, EZH2 forms Polycomb Repressive Complex 2 (PRC2) where it carries on its enzymatic activity of lysin specific DNA methylase *(Schlacher et al, 2011)*. All these factors are required for proper PRC2 complex functionality *(Huang et al, 2014)*. Physiologically, PRC2 mediated epigenetic modifications preserve cell identity and chromatin state during preimplantation embryo development *(Simon and Kingston 2009)*.

In CYP-treated blastocyst, this regulatory mechanism appears disrupted: despite EZH2 upregulation, SUZ12 and Rbbp4 are differentially by 1.52- and 1.7-fold respectively.

PRC2 acts mainly by binding to target genes and depositing H3K27me3, a mark that recruits PRC1 via its CBX subunit. Once recruited, PRC1 ubiquinates 119 Lys of histone 2A inducing chromatin compaction and transcription elongation inhibition *(Schwartz et al 2014)*. Maintaining chromatin conformation is critical as blastomeres undergo rapid cleavage. During S phase of cell cycle, histones modifications became diluted by the incorporation of new, unmodified histones in DNA. PRC2 normally offsets the dilution by propagating H3K27me3 at replication forks *(Hansen et al, 2008)*, keeping DNA methylation levels above the threshold required to preserve a repressive chromatin state

(Xu et al, 2015). Baseline methylation levels are fully restored when cell enters the G1 phase, a step essential for blastomere to progress safely into the next S phase *(Scharf et al, 2009)*.

Literature demonstrates that Rbbp4 downregulation, induced by CYP treatment, reduces Suz12 expression *(Mu et al, 2022)*, leading to a substantial reduction of H3K27me3 levels within about 24 hours *(Petracovici and Bonasio, 2021).* The alteration of these two genes expression can't be compensated by the overexpression alone, resulting in massive deregulation in cell cycle control, protein expression and gene silencing.

Consistent with this observation, our transcriptomic analyses revealed significant alterations in regulating specific cell cycle phases, including Haus2 and Haus9 (mitotic spindle assembly) *(Kraus et al, 2023)*, as well as the G1/S interphase checkpoints E2fb8 *(Wasserman et al, 2020)* and Fbxw7 *(Yada et al, 2004)*. Given the rapid cleavage rate of blastomeres, this PRC2-induced dysregulation amplifies exponentially beyond the capacity of cellular regulatory repair systems, ultimately, driving blastomere apoptosis. This outcome aligns with our immunofluorescence data, which showed a significantly increased cell death rate in CYP blastocysts (Paragraph 4.2).

Regarding pluripotency, proper PRC2 function is essential because H3K27 trimethylation represses differentiation genes, preventing their premature expression in early embryos *(Huang et al, 2014)*. Blastocysts lacking functional EZH2 exhibit upregulation of cell differentiation genes *(Huang et al, 2014)* and display altered germ layer specification *(Chen et al, 2025).*

Finally, recent studies link PRC2 function to the oxidative stress response, as the complex can modulate ROS production and scavenging by regulating environmental antioxidants and metabolic complexes *(Qin et al, 2024)*. Specifically, EZH2 overexpression, matching our findings in CYP blastocysts, promotes promoter methylation that represses *Parp1* expression, thereby reducing PARP levels and PARylation capacity. Because PARP is a key executor of DNA damage repair, cells overexpressing EZH2 become increasingly hypersensitive to redox imbalance-induced cell death *(Tempka et al, 2018).* Another key target repressed by PRC2 when EZH2 is overexpressed is Foxo1 *(Ma et al, 2019)*, which was downregulated in CYP blastocysts. Repression of Foxo1 indirectly downregulates downstream antioxidant enzymes such as CAT and SOD, further compromising cellular redox defence *(Su et al, 2022).*

5. CONCLUSIONS AND FUTURE PERSPECTIVES

In summary, my thesis addresses critical literature gaps regarding the impact of CYP on preimplantation embryo development, demonstrating that this insecticide severely impacts multiple physiological aspect of early embryogenesis.

Specifically, treatment with 1nM CYP induces premature developmental arrest, reducing embryo yields across all major evaluated checkpoints. Embryos that manage to reach blastocyst stage, the final phase of preimplantation embryo development, exhibit reduced quality compared to CTR group, both from a morphologically and molecularly.

Immunofluorescence analyses revealed that CYP-treated blastocysts comprise a lower total number of blastomeres and display a markedly higher cell death rate. This indicates that blastocyst expansion is impaired due to a shortage of developmentally competent cells required to drive structural growth. This hypothesis is fully corroborated by the transcriptomic analyses, which identified 508 DEGs mediating widespread dysregulation of key cellular processes. Among the DEGs, core master regulators specific to preimplantation embryo development, encode components of PRC2 complex. Their disruption leads to board alterations in cell cycle control, protein expression and epigenetic modifications maintenance necessary to prevent the premature activation of differentiation pathways. Collectively, these findings suggest that CYP severely disrupts core cellular processes essential for cell survival, driving blastomeres toward cell death. Blastomeres that partially adapt to insecticide-induced stress fail to preserve the developmental competence needed to sustain embryogenesis. Consequently, overall developmental yields decline, yielding a higher proportion of developmentally delayed or expansion-impaired early blastocysts.

Given the significant of these findings, future studies could adopt a more targeted transcriptional approach by analysing early and expanded CYP-treated blastocysts separately, to dissect the precise the molecular drivers of expansion failure. Furthermore, since the current findings are solely based on transcriptomic variations, future studies must evaluate whether these mRNA alterations translate into corresponding changes at the protein level. Quantitative protein analysis (e.g., Western blot or immunofluorescence) of key emerging targets, such as PRC2 complex subunits, will be essential to validate the proposed molecular mechanisms. Finally, embryo transfer studies using CYP-exposed blastocysts in pseudopregnant female mice could provide valuable insights into how these early molecular and cellular defects affect embryo implantation and subsequent post-implantation development *in vivo*.

Bibliography

Abdou, R.H., Sayed, N., 2019. Antioxidant and anti-inflammatory effects of nanoselenium against cypermethrin-induced liver toxicity. CellBio 8, 53–65. https://doi. org/10.4236/cellbio.2019.84004.

Agbohessi P, Olowo L, Degila B, Houedjissi G, Imorou Toko I, Mandiki SNM, Kestemont P. Comparative assessment of acute toxicity and histological changes in liver of African catfish *Clarias gariepinus* exposed to cotton insecticides. J Environ Sci Health B. 2023;58(1):31-44. doi: 10.1080/03601234.2023.2168445.

Agrawal S, Singh A, Tripathi P, Mishra M, Singh PK, Singh MP. Cypermethrin-induced nigrostriatal dopaminergic neurodegeneration alters the mitochondrial function: a proteomics study. Mol Neurobiol. 2015 Apr;51(2):448-65. doi: 10.1007/s12035-014-8696-7.

Arikan K. Cypermethrin and its metabolite 3-PBA as emerging pollutants: Residues in environmental matrices and in the tissues of the Southern white-breasted hedgehog (Erinaceus concolor L.). Chemosphere. 2026 Apr;399:144893. doi: 10.1016/j.chemosphere.2026.144893.

Barcroft LC, Offenberg H, Thomsen P, Watson AJ. Aquaporin proteins in murine trophectoderm mediate transepithelial water movements during cavitation. Dev Biol. 2003 Apr 15;256(2):342-54. doi: 10.1016/s0012-1606(02)00127-6.

Brander SM, He G, Smalling KL, Denison MS, Cherr GN. The in vivo estrogenic and in vitro anti-estrogenic activity of permethrin and bifenthrin. Environ Toxicol Chem. 2012 Dec;31(12):2848-55. doi: 10.1002/etc.2019.

Brison DR. Apoptosis in mammalian preimplantation embryos: regulation by survival factors. Hum Fertil (Camb). 2000;3(1):36-47. doi: 10.1080/1464727002000198671

Buckley, C.E., St Johnston, D., 2022. Apical–basal polarity and the control of epithelial form and function. Nat. Rev. Mol. Cell Biol. 23, 559–577.

Cabot B, Cabot RA. Chromatin remodeling in mammalian embryos. Reproduction. 2018 Mar;155(3):R147-R158. doi: 10.1530/REP-17-0488.

Cardoso TDN, Stupp P, Rakes M, Martins MB, da Silva Filho JG, Grützmacher AD, Nava DE, Bernardi D, Botton M. Lethal and Sublethal Toxicity of Pesticides Used in Fruit Growing on the Parasitoid Diachasmimorpha longicaudata (Hymenoptera: Braconidae): Implications for Integrated Fruit Fly Management. J Econ Entomol. 2021 Dec 6;114(6):2412-2420. doi: 10.1093/jee/toab176.

Chan CJ, Costanzo M, Ruiz-Herrero T, Mönke G, Petrie RJ, Bergert M, Diz-Muñoz A, Mahadevan L, Hiiragi T. Hydraulic control of mammalian embryo size and cell fate. Nature. 2019 Jul;571(7763):112-116. doi: 10.1038/s41586-019-1309-x

Chen H, Xiao J, Hu G, Zhou J, Xiao H, Wang X. Estrogenicity of organophosphorus and pyrethroid pesticides. J Toxicol Environ Health A. 2002 Oct 11;65(19):1419-35. doi: 10.1080/00984100290071243.

Chen J, Huang B, Zhai X, Xu Z, Sun S, Hu J, Dai X, Chen G, Liang D, Liu L, Zhang M. A conserved function of EZH2-PRC2 in repression of primitive endoderm fate in mouse and human pluripotent cells. Stem Cell Reports. 2025 Nov 11;20(11):102689. doi: 10.1016/j.stemcr.2025.102689.

Choudhary GS, Al-Harbi S, Almasan A. Caspase-3 activation is a critical determinant of genotoxic stress-induced apoptosis. Methods Mol Biol. 2015;1219:1-9. doi: 10.1007/978-1-4939-1661-0_1.

Clark JM, Symington SB. Advances in the mode of action of pyrethroids. Top Curr Chem. 2012;314:49-72. doi: 10.1007/128_2011_268. PMID: 22025067.

De Gavelle E, de Lauzon-Guillain B, Charles MA, Chevrier C, Hulin M, Sirot V, Merlo M, Nougadère A. Chronic dietary exposure to pesticide residues and associated risk in the French ELFE cohort of pregnant women. Environ Int. 2016 Jul-Aug;92-93:533-42. doi: 10.1016/j.envint.2016.04.007.

Diaz de Cerio O, Rojo-Bartolomé I, Bizarro C, Ortiz-Zarragoitia M, Cancio I. 5S rRNA and accompanying proteins in gonads: powerful markers to identify sex and reproductive endocrine disruption in fish. Environ Sci Technol. 2012 Jul 17;46(14):7763-71. doi: 10.1021/es301132b

Dietrich JE, Hiiragi T. Stochastic patterning in the mouse pre-implantation embryo. Development. 2007 Dec;134(23):4219-31. doi: 10.1242/dev.003798.

Dumay-Odelot H, Durrieu-Gaillard S, Da Silva D, Roeder RG, Teichmann M. Cell growth- and differentiation-dependent regulation of RNA polymerase III transcription. Cell Cycle. 2010 Sep 15;9(18):3687-99. doi: 10.4161/cc.9.18.13203

Dumollard R, Minc N, Salez G, Aicha SB, Bekkouche F, Hebras C, Besnardeau L, McDougall A. The invariant cleavage pattern displayed by ascidian embryos depends on spindle positioning along the cell's longest axis in the apical plane and relies on asynchronous cell divisions. Elife. 2017 Jan 25;6:e19290. doi: 10.7554/eLife.19290.

Elsawy H, Al-Omair MA, Sedky A, Al-Otaibi L. Protective effect of α-lipoic acid against α-cypermethrin-induced changes in rat cerebellum. J Chem Neuroanat. 2017 Dec;86:52-58. doi: 10.1016/j.jchemneu.2017.08.005.

Elston R, Inman GJ. Crosstalk between p53 and TGF-β Signalling. J Signal Transduct. 2012;2012:294097. doi: 10.1155/2012/294097.

Engelke DR, Ng SY, Shastry BS, Roeder RG. Specific interaction of a purified transcription factor with an internal control region of 5S RNA genes. Cell. 1980 Mar;19(3):717-28. doi: 10.1016/s0092-8674(80)80048-1

Environmental Protection Agency (U.S. EPA). Reregistration eligibility decision for cypermethrin. 2006. Available from: http://www.epa.gov/oppsrrd1/REDs/cypermethrin_red.pdf. Accessed May 26, 2009

European Food Safety Authority (EFSA). Conclusion regarding the peer review of the pesticide risk assessment of the active substance zeta-cypermethrin. *EFSA Sci Rep.* 2008;196:1–119.

European Union Directive. Directive 2009/128/EC of the European Parliament and of the Council of 21 October 2009 establishing a framework for Community action. 2009. Available from: https://eur-lex.europa.eu/legal-content/EN/ALL/?uri=CELEX%3A32009L0128.

Evans MJ, Kaufman MH. Establishment in culture of pluripotential cells from mouse embryos. Nature. 1981 Jul 9;292(5819):154-6. doi: 10.1038/292154a0.

Fetoui H, Makni M, Garoui el M, Zeghal N. Toxic effects of lambda-cyhalothrin, a synthetic pyrethroid pesticide, on the rat kidney: Involvement of oxidative stress and protective role of ascorbic acid. Exp Toxicol Pathol. 2010 Nov;62(6):593-9. doi: 10.1016/j.etp.2009.08.004.

Fierro-González JC, White MD, Silva JC, Plachta N. Cadherin-dependent filopodia control preimplantation embryo compaction. Nat Cell Biol. 2013 Dec;15(12):1424-33. doi: 10.1038/ncb2875.

Food and Agriculture Organization of the United Nations. International code of conduct on the distribution and use of pesticides. 2002:36. [cited 2018 Apr 7]. Available from: http://www.fao.org/docrep/005/y5544e/y4544e00.htm

Frum T, Murphy TM, Ralston A. HIPPO signaling resolves embryonic cell fate conflicts during establishment of pluripotency in vivo. Elife. 2018 Dec 11;7:e42298. doi: 10.7554/eLife.42298.

Gaarenstroom T, Hill CS. TGF-β signallingto chromatin: how Smads regulate transcription during self-renewal and differentiation. Semin Cell Dev Biol. 2014 Aug;32:107-18. doi: 10.1016/j.semcdb.2014.01.009.

Gan J, Lee SJ, Liu WP, Haver DL, Kabashima JN. Distribution and persistence of pyrethroids in runoff sediments. J Environ Qual. 2005 Apr 20;34(3):836-41. doi: 10.2134/jeq2004.0240.

Garoussi, M. T., Sasani, F., & Hovareshti, P. (2010). The histopathological survey of uterine tissue in holstein dairy cows with or without recorded reproductive disorders. *Iranian Journal of Veterinary Science and Technology*, *2*(2), 101-108.

Gill SA, Rizvi F, Khan MZ, Khan A. Toxic effects of cypermethrin and methamidophos on bovine corpus luteal cells and progesterone production. Exp Toxicol Pathol. 2011 Jan;63(1-2):131-5. doi: 10.1016/j.etp.2009.10.007.

GOI (2020). *Statistical Database*. Directorate of Plant Protection, Quarantine & Storage, Government of India. Available from: http://ppqs.gov.in/statistical%20database

Grewal KK, Sandhu GS, Kaur R, Brar RS, Sandhu HS. Toxic impacts of cypermethrin on behavior and histology of certain tissues of albino rats. Toxicol Int. 2010 Jul;17(2):94-8. doi: 10.4103/0971-6580.72679.

Gu B, Bradshaw B, Zhu M, Sun Y, Hopyan S, Rossant J. Live imaging YAP signalling in mouse embryo development. Open Biol. 2022 Jan;12(1):210335. doi: 10.1098/rsob.210335.

Guo G, Wang W, Tu M, Zhao B, Han J, Li J, Pan Y, Zhou J, Ma W, Liu Y, Sun T, Han X, An Y. Deciphering adipose development: Function, differentiation and regulation. Dev Dyn. 2024 Nov;253(11):956-997. doi: 10.1002/dvdy.708.

Guzman L, Nuñez D, López R, Inoue N, Portella J, Vizcarra F, Noriega-Portella L, Noriega-Hoces L, Munné S. The number of biopsied trophectoderm cells may affect pregnancy outcomes. J Assist Reprod Genet. 2019 Jan;36(1):145-151. doi: 10.1007/s10815-018-1331-1

Hagen T. Oxygen versus Reactive Oxygen in the Regulation of HIF-1α: The Balance Tips. Biochem Res Int. 2012;2012:436981. doi: 10.1155/2012/436981

Hansen KH, Bracken AP, Pasini D, Dietrich N, Gehani SS, Monrad A, Rappsilber J, Lerdrup M, Helin K. A model for transmission of the H3K27me3 epigenetic mark. Nat Cell Biol. 2008 Nov;10(11):1291-300. doi: 10.1038/ncb1787.

Hassig CA, Fleischer TC, Billin AN, Schreiber SL, Ayer DE. Histone deacetylase activity is required for full transcriptional repression by mSin3A. Cell. 1997 May 2;89(3):341-7. doi: 10.1016/s0092-8674(00)80214-7.

He Q, Zhang X, Yang X. Glutathione mitigates meiotic defects in porcine oocytes exposed to beta-cypermethrin by regulating ROS levels. Toxicology. 2023 Aug 1;494:153592. doi: 10.1016/j.tox.2023.153592.

Hirate Y, Hirahara S, Inoue K, Suzuki A, Alarcon VB, Akimoto K, Hirai T, Hara T, Adachi M, Chida K, Ohno S, Marikawa Y, Nakao K, Shimono A, Sasaki H. Polarity-dependent distribution of angiomotin localizes Hippo signaling in preimplantation embryos. Curr Biol. 2013 Jul 8;23(13):1181-94. doi: 10.1016/j.cub.2013.05.014.

Huang XJ, Wang X, Ma X, Sun SC, Zhou X, Zhu C, Liu H. EZH2 is essential for development of mouse preimplantation embryos. Reprod Fertil Dev. 2014 Oct;26(8):1166-75. doi: 10.1071/RD13169.

Hussain S, Ashafaq M, Alshahrani S, Bokar IAM, Siddiqui R, Alam MI, Taha MME, Almoshari Y, Alqahtani SS, Ahmed RA, Jali AM, Qadri M. Hepatoprotective Effect of Curcumin Nano-Lipid Carrier against Cypermethrin Toxicity by Countering the Oxidative, Inflammatory, and Apoptotic Changes in Wistar Rats. Molecules. 2023 Jan 16;28(2):881. doi: 10.3390/molecules28020881.

Ismail, B.S., Mazlinda, M., Tayeb, M.A., 2013. Adsorption, desorption and mobility of cypermethrin and deltamethrin in Malaysian soils. Inter. J. Plant Animal Environ. Sci. 3, 23–29. MANCA SU PUBMED

Jaensson A, Scott AP, Moore A, Kylin H, Olsén KH. Effects of a pyrethroid pesticide on endocrine responses to female odours and reproductive behaviour in male parr of brown trout (Salmo trutta L.). Aquat Toxicol. 2007 Feb 15;81(1):1-9. doi: 10.1016/j.aquatox.2006.10.011.

Kalyabina VP, Esimbekova EN, Kopylova KV, Kratasyuk VA. Pesticides: formulants, distribution pathways and effects on human health - a review. Toxicol Rep. 2021 Jun 6;8:1179-1192. doi: 10.1016/j.toxrep.2021.06.004.

Kansal I, Kapoor A, Solanki S, Singh R. Cypermethrin toxicity in the environment: analytical insight into detection methods and microbial degradation pathways. J Appl Microbiol. 2023 Jun 1;134(6):lxad105. doi: 10.1093/jambio/lxad105.

Kassavetis GA, Braun BR, Nguyen LH, Geiduschek EP. S. cerevisiae TFIIIB is the transcription initiation factor proper of RNA polymerase III, while TFIIIA and TFIIIC are assembly factors. Cell. 1990 Jan 26;60(2):235-45. doi: 10.1016/0092-8674(90)90739-2.

Kašuba V, Tariba Lovaković B, Lucić Vrdoljak A, Katić A, Kopjar N, Micek V, Milić M, Pizent A, Želježić D, Žunec S. Evaluation of Toxic Effects Induced by Sub-Acute Exposure to Low Doses of α-Cypermethrin in Adult Male Rats. Toxics. 2022 Nov 23;10(12):717. doi: 10.3390/toxics10120717.

Kawagishi R, Tahara M, Sawada K, Morishige K, Sakata M, Tasaka K, Murata Y. Na+ / H+ exchanger-3 is involved in mouse blastocyst formation. J Exp Zool A Comp Exp Biol. 2004 Sep 1;301(9):767-75. doi: 10.1002/jez.a.90.

Kerr JF, Wyllie AH, Currie AR. Apoptosis: a basic biological phenomenon with wide-ranging implications in tissue kinetics. Br J Cancer. 1972 Aug;26(4):239-57. doi: 10.1038/bjc.1972.33.

Khan T, Waseem R, Zehra Z, Aiman A, Bhardwaj P, Ansari J, Hassan MI, Islam A. Mitochondrial Dysfunction: Pathophysiology and Mitochondria-Targeted Drug Delivery Approaches. Pharmaceutics. 2022 Nov 30;14(12):2657. doi: 10.3390/pharmaceutics14122657. PMID: 36559149; PMCID: PMC9785072.

Kim YS, Bedzhov I. Mechanisms of formation and functions of the early embryonic cavities. Semin Cell Dev Biol. 2022 Nov;131:110-116. doi: 10.1016/j.semcdb.2022.04.020.

Korotkevich E, Niwayama R, Courtois A, Friese S, Berger N, Buchholz F, Hiiragi T. The Apical Domain Is Required and Sufficient for the First Lineage Segregation in the Mouse Embryo. Dev Cell. 2017 Feb 6;40(3):235-247.e7. doi: 10.1016/j.devcel.2017.01.006.

Kraus J, Travis SM, King MR, Petry S. Augmin is a Ran-regulated spindle assembly factor. J Biol Chem. 2023 Jun;299(6):104736. doi: 10.1016/j.jbc.2023.104736.

Krawczyk K, Wilczak K, Szczepańska K, Maleszewski M, Suwińska A. Paracrine interactions through FGFR1 and FGFR2 receptors regulate the development of preimplantation mouse chimaeric embryo. Open Biol. 2022 Nov;12(11):220193. doi: 10.1098/rsob.220193.

Kurowski A, Molotkov A, Soriano P. FGFR1 regulates trophectoderm development and facilitates blastocyst implantation. Dev Biol. 2019 Feb 1;446(1):94-101. doi: 10.1016/j.ydbio.2018.12.008.

Le Verge-Serandour M, Turlier H. Blastocoel morphogenesis: A biophysics perspective. Semin Cell Dev Biol. 2022 Oct;130:12-23. doi: 10.1016/j.semcdb.2021.10.005.

Li D, Chen L, Cai X, Qi Y, Lu Y. Comparative Population Biology and Related Gene Expression in the Beta-Cypermethrin-Resistant Strains of *Bactrocera dorsalis* (Hendel). Insects. 2024 Jul 26;15(8):569. doi: 10.3390/insects15080569.

Liu-Chittenden Y, Huang B, Shim JS, Chen Q, Lee SJ, Anders RA, Liu JO, Pan D. Genetic and pharmacological disruption of the TEAD-YAP complex suppresses the oncogenic activity of YAP. Genes Dev. 2012 Jun 15;26(12):1300-5. doi: 10.1101/gad.192856.112.

Luzzani C, Solari C, Losino N, Ariel W, Romorini L, Bluguermann C, Sevlever G, Barañao L, Miriuka S, Guberman A. Modulation of chromatin modifying factors' gene expression in embryonic and induced pluripotent stem cells. Biochem Biophys Res Commun. 2011 Jul 15;410(4):816-22. doi: 10.1016/j.bbrc.2011.06.070

Ma L, Yan Y, Bai Y, Yang Y, Pan Y, Gang X, Karnes RJ, Zhang J, Lv Q, Wu Q, Huang H. Overcoming EZH2 Inhibitor Resistance by Taxane in PTEN-Mutated Cancer. Theranostics. 2019 Jul 9;9(17):5020-5034. doi: 10.7150/thno.34700.

Madan P, Rose K, Watson AJ. Na/K-ATPase beta1 subunit expression is required for blastocyst formation and normal assembly of trophectoderm tight junction-associated proteins. J Biol Chem. 2007 Apr 20;282(16):12127-34. doi: 10.1074/jbc.M700696200.

Mahadevan M, Baker G. Assessment and preparation of semen for in vitro fertilization. In: Wood C, Trounson A, editors. Clinical in vitro fertilization. London: Springer; 1984. doi: 10.1007/978-1-4471-3317-9_7.

Maître JL, Niwayama R, Turlier H, Nédélec F, Hiiragi T. Pulsatile cell-autonomous contractility drives compaction in the mouse embryo. Nat Cell Biol. 2015 Jul;17(7):849-55. doi: 10.1038/ncb3185. Epub 2015 Jun 15. Erratum in: Nat Cell Biol. 2017 Jul 28;19(8):1003. doi: 10.1038/ncb3587.

Majumder, R., Kaviraj, A., 2022. Histopathological alterations of gills, liver and kidney of freshwater fish, Oreochromis niloticus, exposed to cypermethrin. J. Aquat. Biol. Fish. 10 (1), 1–5.

Marchi S, Patergnani S, Missiroli S, Morciano G, Rimessi A, Wieckowski MR, Giorgi C, Pinton P. Mitochondrial and endoplasmic reticulum calcium homeostasis and cell death. Cell Calcium. 2018 Jan;69:62-72. doi: 10.1016/j.ceca.2017.05.003.

Marettova E, Maretta M, Legáth J. Effect of pyrethroids on female genital system. Review. Anim Reprod Sci. 2017 Sep;184:132-138. doi: 10.1016/j.anireprosci.2017.07.007.

Merico V, Zanoni M, Parada-Bustamante A, Garagna S, Zuccotti M. In Vitro Maturation of Fully Grown Mouse Antral Follicles in the Presence of 1 nM 2-Hydroxyestradiol Improves Oocytes' Developmental Competence. Reprod Sci. 2021 Jan;28(1):121-133. doi: 10.1007/s43032-020-00276-6.

Mitsui K, Tokuzawa Y, Itoh H, Segawa K, Murakami M, Takahashi K, Maruyama M, Maeda M, Yamanaka S. The homeoprotein Nanog is required for maintenance of pluripotency in mouse epiblast and ES cells. Cell. 2003 May 30;113(5):631-42. doi: 10.1016/s0092-8674(03)00393-3.

Mu W, Murcia NS, Smith KN, Menon DU, Yee D, Magnuson T. RBBP4 dysfunction reshapes the genomic landscape of H3K27 methylation and acetylation and disrupts gene expression. G3 (Bethesda). 2022 May 30;12(6):jkac082. doi: 10.1093/g3journal/jkac082.

Namdev, N., Rai, G., Mahobiya, P., 2023. Preventive role of dietary antioxidants against cypermethrin-induced toxicological effects: ashwagandha and quercetin. Goya J. 16 (5), 325–334 doi: 12.163022.Gj.2023.v16.05.0046.

Naserabad SS, Zarei S, Rahimi J, Ghafouri Z, Mouludi-Saleh A, Banaee M. Protective effects of Allium jesdianum essential oil on rainbow trout (Oncorhynchus mykiss) exposed to sub-lethal toxicity of cypermethrin. Aquat Toxicol. 2024 Sep;274:107051. doi: 10.1016/j.aquatox.2024.107051.

Ng RK, Dean W, Dawson C, Lucifero D, Madeja Z, Reik W, Hemberger M. Epigenetic restriction of embryonic cell lineage fate by methylation of Elf5. Nat Cell Biol. 2008 Nov;10(11):1280-90. doi: 10.1038/ncb1786.

Ni FD, Hao SL, Yang WX. Multiple signaling pathways in Sertoli cells: recent findings in spermatogenesis. Cell Death Dis. 2019 Jul 17;10(8):541. doi: 10.1038/s41419-019-1782-z.

Nichols J, Zevnik B, Anastassiadis K, Niwa H, Klewe-Nebenius D, Chambers I, Schöler H, Smith A. Formation of pluripotent stem cells in the mammalian embryo depends on the POU transcription factor Oct4. Cell. 1998 Oct 30;95(3):379-91. doi: 10.1016/s0092-8674(00)81769-9.

Nishioka N, Inoue K, Adachi K, Kiyonari H, Ota M, Ralston A, Yabuta N, Hirahara S, Stephenson RO, Ogonuki N, Makita R, Kurihara H, Morin-Kensicki EM, Nojima H, Rossant J, Nakao K, Niwa H, Sasaki H. The Hippo signaling pathway components Lats and Yap pattern Tead4 activity to distinguish mouse trophectoderm from inner cell mass. Dev Cell. 2009 Mar;16(3):398-410. doi: 10.1016/j.devcel.2009.02.003.

Petracovici A, Bonasio R. Distinct PRC2 subunits regulate maintenance and establishment of Polycomb repression during differentiation. Mol Cell. 2021 Jun 17;81(12):2625-2639.e5. doi: 10.1016/j.molcel.2021.03.038.

Pfeffer PL. The first lineage determination in mammals. Dev Biol. 2024 Sep;513:12-30. doi: 10.1016/j.ydbio.2024.05.011.

Prasamthi K, Muralidhara, Rajini PS. Fenvalerate-induced oxidative damage in rat tissues and its attenuation by dietary sesame oil. Food Chem Toxicol. 2005 Feb;43(2):299-306. doi: 10.1016/j.fct.2004.10.005

Promthep K, Nopparat C, Mukda S, Pannengpetch S, Wisomka P, Chantadul V, Phanchana M, Panmanee J. Proteomic profiling reveals neuronal ion channel dysregulation and cellular responses to DNA damage-induced cell cycle arrest and senescence in human neuroblastoma SH-SY5Y cells exposed to cypermethrin. Neurotoxicology. 2022 Dec;93:71-83. doi: 10.1016/j.neuro.2022.08.015.

Qin H, Liu C, Li C, Feng C, Bo Huang. Advances in bi-directional relationships for EZH2 and oxidative stress. Exp Cell Res. 2024 Jan 1;434(1):113876. doi: 10.1016/j.yexcr.2023.113876.

Qu X, Zou Z, Sun Q, Luby-Phelps K, Cheng P, Hogan RN, Gilpin C, Levine B. Autophagy gene-dependent clearance of apoptotic cells during embryonic development. Cell. 2007 Mar 9;128(5):931-46. doi: 10.1016/j.cell.2006.12.044.

Ralston, A., Rossant, J., 2008. Cdx2 acts downstream of cell polarization to cell-autonomously promote trophectoderm fate in the early mouse embryo. Dev. Biol. 313, 614–629.

Rebuzzini P, Civello C, Nantia Akono E, Fassina L, Zuccotti M, Garagna S. Chronic cypermethrin exposure alters mouse embryonic stem cell growth kinetics, induces Phase II detoxification response and affects pluripotency and differentiation gene expression. Eur J Histochem. 2020 Feb 17;64(1):3084. doi: 10.4081/ejh.2020.3084.

Rizzino A, Wuebben EL. Sox2/Oct4: A delicately balanced partnership in pluripotent stem cells and embryogenesis. Biochim Biophys Acta. 2016 Jun;1859(6):780-91. doi: 10.1016/j.bbagrm.2016.03.006.

Russ AP, Wattler S, Colledge WH, Aparicio SA, Carlton MB, Pearce JJ, Barton SC, Surani MA, Ryan K, Nehls MC, Wilson V, Evans MJ. Eomesodermin is required for mouse trophoblast development and mesoderm formation. Nature. 2000 Mar 2;404(6773):95-9. doi: 10.1038/35003601.

Saka WA, Akhigbe RE, Azeez OM, Babatunde TR. Effects of pyrethroid insecticide exposure on haematological and haemostatic profiles in rats. Pak J Biol Sci. 2011 Nov 15;14(22):1024-7. doi: 10.3923/pjbs.2011.1024.1027.

Sangha GK, Kaur K, Khera KS. Cypermethrin induced pathological and biochemical changes in reproductive organs of female rats. J Environ Biol. 2013 Jan;34(1):99-105.

Sasaki H. Mechanisms of trophectoderm fate specification in preimplantation mouse development. Dev Growth Differ. 2010 Apr;52(3):263-73. doi: 10.1111/j.1440-169X.2009.01158.x.

Scharf AN, Barth TK, Imhof A. Establishment of histone modifications after chromatin assembly. Nucleic Acids Res. 2009 Aug;37(15):5032-40. doi: 10.1093/nar/gkp518.

Schlacher K, Christ N, Siaud N, Egashira A, Wu H, Jasin M. Double-strand break repair-independent role for BRCA2 in blocking stalled replication fork degradation by MRE11. Cell. 2011 May 13;145(4):529-42. doi: 10.1016/j.cell.2011.03.041

Schreinemachers P, Chen HP, Nguyen TTL, Buntong B, Bouapao L, Gautam S, Le NT, Pinn T, Vilaysone P, Srinivasan R. Too much to handle? Pesticide dependence of smallholder vegetable farmers in Southeast Asia. Sci Total Environ. 2017 Sep 1;593-594:470-477. doi: 10.1016/j.scitotenv.2017.03.181.

Schulz KN, Harrison MM. Mechanisms regulating zygotic genome activation. Nat Rev Genet. 2019 Apr;20(4):221-234. doi: 10.1038/s41576-018-0087-x.

Schwartz YB, Pirrotta V. Ruled by ubiquitylation: a new order for polycomb recruitment. Cell Rep. 2014 Jul 24;8(2):321-5. doi: 10.1016/j.celrep.2014.07.001.

Seifart KH, Wang L, Waldschmidt R, Jahn D, Wingender E. Purification of human transcription factor IIIA and its interaction with a chemically synthesized gene encoding human 5 S rRNA. J Biol Chem. 1989 Jan 25;264(3):1702-9.

Sfakianoudis K, Maziotis E, Karantzali E, Kokkini G, Grigoriadis S, Pantou A, Giannelou P, Petroutsou K, Markomichali C, Fakiridou M, Koutsilieris M, Asimakopoulos B, Pantos K, Simopoulou M. Molecular Drivers of Developmental Arrest in the Human Preimplantation Embryo: A Systematic Review and Critical Analysis Leading to Mapping Future Research. Int J Mol Sci. 2021 Aug 3;22(15):8353. doi: 10.3390/ijms22158353.

Sharma R, Jindal R, Faggio C. Impact of cypermethrin in nephrocytes of freshwater fish Catla catla. Environ Toxicol Pharmacol. 2021 Nov;88:103739. doi: 10.1016/j.etap.2021.103739.

Silva, D. M. L. D., Camargo, P. B. D., Martinelli, L. A., Lancas, F. M., Pinto, J. S., & Avelar, W. E. P. (2008). Organochlorine pesticides in Piracicaba river basin (Sao Paulo/Brazil): A survey of sediment, bivalve and fish. *Quimica Nova, 31*, 214–219. MANCA SU PUBMED

Simon JA, Kingston RE. Mechanisms of polycomb gene silencing: knowns and unknowns. Nat Rev Mol Cell Biol. 2009 Oct;10(10):697-708. doi: 10.1038/nrm2763.

Sinha V, Shrivastava S. Cypermethrin: An Emerging Pollutant and Its Adverse Effect on Fish Health and some Preventive Approach-A Review. Indian J Microbiol. 2024 Mar;64(1):48-58. doi: 10.1007/s12088-023-01153-x.

Smith A. The battlefield of pluripotency. Cell. 2005 Dec 2;123(5):757-60. doi: 10.1016/j.cell.2005.11.012.

Soderlund DM, Clark JM, Sheets LP, Mullin LS, Piccirillo VJ, Sargent D, Stevens JT, Weiner ML. Mechanisms of pyrethroid neurotoxicity: implications for cumulative risk assessment. Toxicology. 2002 Feb 1;171(1):3-59. doi: 10.1016/s0300-483x(01)00569-8.

Soltanian S, Fereidouni MS. Immunotoxic responses of chronic exposure to cypermethrin in common carp. Fish Physiol Biochem. 2017 Dec;43(6):1645-1655. doi: 10.1007/s10695-017-0399-3.

Spies M, Fishel R. Mismatch repair during homologous and homeologous recombination. Cold Spring Harb Perspect Biol. 2015 Mar 2;7(3):a022657. doi: 10.1101/cshperspect.a022657.

Sritanaudomchai H, Sparman M, Tachibana M, Clepper L, Woodward J, Gokhale S, Wolf D, Hennebold J, Hurlbut W, Grompe M, Mitalipov S. CDX2 in the formation of the trophectoderm lineage in primate embryos. Dev Biol. 2009 Nov 1;335(1):179-87. doi: 10.1016/j.ydbio.2009.08.025.

Stirparo GG, Kurowski A, Yanagida A, Bates LE, Strawbridge SE, Hladkou S, Stuart HT, Boroviak TE, Silva JCR, Nichols J. OCT4 induces embryonic pluripotency via STAT3 signaling and metabolic mechanisms. Proc Natl Acad Sci U S A. 2021 Jan 19;118(3):e2008890118. doi: 10.1073/pnas.2008890118.

Strumpf D, Mao CA, Yamanaka Y, Ralston A, Chawengsaksophak K, Beck F, Rossant J. Cdx2 is required for correct cell fate specification and differentiation of trophectoderm in the mouse blastocyst. Development. 2005 May;132(9):2093-102. doi: 10.1242/dev.01801.

Su X, Zhang H, Lei F, Wang R, Lin T, Liao L. Epigenetic therapy attenuates oxidative stress in BMSCs during ageing. J Cell Mol Med. 2022 Jan;26(2):375-384. doi: 10.1111/jcmm.17089.

Suarez-Huerta N, Mosselmans R, Dumont JE, Robaye B. Actin depolymerization and polymerization are required during apoptosis in endothelial cells. J Cell Physiol. 2000 Aug;184(2):239-45. doi: 10.1002/1097-4652(200008)184:2<239::AID-JCP12>3.0.CO;2-R.

Sun H, Chen W, Xu X, Ding Z, Chen X, Wang X. Pyrethroid and their metabolite, 3-phenoxybenzoic acid showed similar (anti)estrogenic activity in human and rat estrogen receptor α-mediated reporter gene assays. Environ Toxicol Pharmacol. 2014 Jan;37(1):371-7. doi: 10.1016/j.etap.2013.11.031.

Sun J, Li J, Wang Y, Qu J, Bi F, Xiang H, Zhao X, Sun M, Huan Y. Astaxanthin protects oocyte maturation against cypermethrin-induced defects in pigs. Theriogenology. 2023 Oct 1;209:31-39. doi: 10.1016/j.theriogenology.2023.06.022.

Swain N, Thakur M, Pathak J, Swain B. SOX2, OCT4 and NANOG: The core embryonic stem cell pluripotency regulators in oral carcinogenesis. J Oral Maxillofac Pathol. 2020 May-Aug;24(2):368-373. doi: 10.4103/jomfp.JOMFP_22_20.

Tadros W, Lipshitz HD. The maternal-to-zygotic transition: a play in two acts. Development. 2009 Sep;136(18):3033-42. doi: 10.1242/dev.033183.

Tempka D, Tokarz P, Chmielewska K, Kluska M, Pietrzak J, Rygielska Ż, Virág L, Robaszkiewicz A. Downregulation of PARP1 transcription by CDK4/6 inhibitors sensitizes human lung cancer cells to anticancer drug-induced death by impairing OGG1-dependent base excision repair. Redox Biol. 2018 May;15:316-326. doi: 10.1016/j.redox.2017.12.017.

Thoudam T, Ha CM, Leem J, Chanda D, Park JS, Kim HJ, Jeon JH, Choi YK, Liangpunsakul S, Huh YH, Kwon TH, Park KG, Harris RA, Park KS, Rhee HW, Lee IK. PDK4 Augments ER-Mitochondria Contact to Dampen Skeletal Muscle Insulin Signaling During Obesity. Diabetes. 2019 Mar;68(3):571-586. doi: 10.2337/db18-0363.

Totaro A, Panciera T, Piccolo S. YAP/TAZ upstream signals and downstream responses. Nat Cell Biol. 2018 Aug;20(8):888-899. doi: 10.1038/s41556-018-0142-z.

Tudi M, Ruan HD, Wang L, et al. Agriculture development, pesticide application and its impact on the environment. *Int J Environ Res Public Health.* 2021 Feb;18(3):1112. doi:10.3390/ijerph18031112.

Ullah S, Li Z, Ul Arifeen MZ, Khan SU, Fahad S. Multiple biomarkers based appraisal of deltamethrin induced toxicity in silver carp (Hypophthalmichthys molitrix). Chemosphere. 2019 Jan;214:519-533. doi: 10.1016/j.chemosphere.2018.09.145.

Ullah, M. S., Ahmad, M., Ahmad, N., Khan, M. Z., & Ahmad, I. (2006). Toxic effects of cypermethrin in female rabbits. *Pakistan veterinary journal*, *26*(4), 193.

Valencia A, Rojo-Bartolomé I, Bizarro C, Cancio I, Ortiz-Zarragoitia M. Alteration in molecular markers of oocyte development and intersex condition in mullets impacted by wastewater treatment plant effluents. Gen Comp Endocrinol. 2017 May 1;245:10-18. doi: 10.1016/j.ygcen.2016.06.017

Vinot S, Le T, Ohno S, Pawson T, Maro B, Louvet-Vallée S. Asymmetric distribution of PAR proteins in the mouse embryo begins at the 8-cell stage during compaction. Dev Biol. 2005 Jun 15;282(2):307-19. doi: 10.1016/j.ydbio.2005.03.001.

Wang Q, Shen JY, Zhang R, Hong JW, Li Z, Ding Z, Wang HX, Zhang JP, Zhang MR, Xu LC. Effects and mechanisms of pyrethroids on male reproductive system. Toxicology. 2020 May 30;438:152460. doi: 10.1016/j.tox.2020.152460.

Wasserman D, Nachum S, Cohen M, Enrico TP, Noach-Hirsh M, Parasol J, Zomer-Polak S, Auerbach N, Sheinberger-Chorni E, Nevenzal H, Levi-Dadon N, Wang X, Lahmi R, Michaely E, Gerber D, Emanuele MJ, Tzur A. Cell cycle oscillators underlying orderly proteolysis of E2F8. Mol Biol Cell. 2020 Apr 1;31(8):725-740. doi: 10.1091/mbc

Watanabe T, Biggins JS, Tannan NB, Srinivas S. Limited predictive value of blastomere angle of division in trophectoderm and inner cell mass specification. Development. 2014 Jun;141(11):2279-88. doi: 10.1242/dev.103267.

Watson AJ, Natale DR, Barcroft LC. Molecular regulation of blastocyst formation. Anim Reprod Sci. 2004 Jul;82-83:583-92. doi: 10.1016/j.anireprosci.2004.04.004.

Wicklow E, Blij S, Frum T, Hirate Y, Lang RA, Sasaki H, Ralston A. HIPPO pathway members restrict SOX2 to the inner cell mass where it promotes ICM fates in the mouse blastocyst. PLoS Genet. 2014 Oct 23;10(10):e1004618. doi: 10.1371/journal.pgen.1004618.

Wielgomas B, Krechniak J (2007) Effect of α-cypermethrin and chlorpyrifos in a 28-day study on free radical parameters and cholinesterase activity in Wistar rats. Pol J Environ Stud 16:91–95 (non c'è su pubmed, Sinha ecc è l'articolo di riferimento)

World Health Organization. Deltamethrin long-lasting (coated onto filaments) insecticidal net. (s)α-Cyano-3-phenoxybenzyl (1r,3r)-3-(2,2-dibromovinyl)-2,2-dimethylcyclopropane carboxylate. Geneva: World Health Organization; 2017.

Xu M, Wang W, Chen S, Zhu B. A model for mitotic inheritance of histone lysine methylation. EMBO Rep. 2011 Dec 23;13(1):60-7. doi: 10.1038/embor.2011.206.

Xue Y, Wong J, Moreno GT, Young MK, Côté J, Wang W. NURD, a novel complex with both ATP-dependent chromatin-remodeling and histone deacetylase activities. Mol Cell. 1998 Dec;2(6):851-61. doi: 10.1016/s1097-2765(00)80299-3.

Yada M, Hatakeyama S, Kamura T, Nishiyama M, Tsunematsu R, Imaki H, Ishida N, Okumura F, Nakayama K, Nakayama KI. Phosphorylation-dependent degradation of c-Myc is mediated by the F-box protein Fbw7. EMBO J. 2004 May 19;23(10):2116-25. doi: 10.1038/sj.emboj.7600217.

You A, Tong JK, Grozinger CM, Schreiber SL. CoREST is an integral component of the CoREST-human histone deacetylase complex. Proc Natl Acad Sci U S A. 2001 Feb 13;98(4):1454-8. doi: 10.1073/pnas.98.4.1454.

Young RA. Control of the embryonic stem cell state. Cell. 2011 Mar 18;144(6):940-54. doi: 10.1016/j.cell.2011.01.032.

Zenker, J., White, M.D., Gasnier, M., Alvarez, Y.D., Lim, H.Y.G., Bissiere, S., Biro, M., Plachta, N., 2018. Expanding actin rings zipper the mouse embryo for blastocyst formation. Cell 173, 776–791.e717.

Zhang C, Wang JJ, He X, Wang C, Zhang B, Xu J, Xu W, Luo Y, Huang K. Characterization and Beige Adipogenic Potential of Human Embryo White Adipose Tissue-Derived Stem Cells. Cell Physiol Biochem. 2018;51(6):2900-2915. doi: 10.1159/000496042

Zhang CY, Yang M. Roles of fibroblast growth factors in the treatment of diabetes. World J Diabetes. 2024 Mar 15;15(3):392-402. doi: 10.4239/wjd.v15.i3.392.

Zhang R, Wang XX, Xie JF, Yao TT, Guo QW, Wang Q, Ding Z, Zhang JP, Zhang MR, Xu LC. Cypermethrin induces Sertoli cell apoptosis through endoplasmic reticulum-mitochondrial coupling involving IP3R1-GRP75-VDAC1. Reprod Toxicol. 2024 Mar;124:108552. doi: 10.1016/j.reprotox.2024.108552.

Zhao B, Wei X, Li W, Udan RS, Yang Q, Kim J, Xie J, Ikenoue T, Yu J, Li L, Zheng P, Ye K, Chinnaiyan A, Halder G, Lai ZC, Guan KL. Inactivation of YAP oncoprotein by the Hippo pathway is involved in cell contact inhibition and tissue growth control. Genes Dev. 2007 Nov 1;21(21):2747-61. doi: 10.1101/gad.1602907.

Zhu M, Cornwall-Scoones J, Wang P, Handford CE, Na J, Thomson M, Zernicka-Goetz M. Developmental clock and mechanism of de novo polarization of the mouse embryo. Science. 2020 Dec 11;370(6522):eabd2703. doi: 10.1126/science.abd2703.

Zhu M, Leung CY, Shahbazi MN, Zernicka-Goetz M. Actomyosin polarisation through PLC-PKC triggers symmetry breaking of the mouse embryo. Nat Commun. 2017 Oct 13;8(1):921. doi: 10.1038/s41467-017-00977-8.

Zhu, M., Cornwall-Scoones, J., Wang, P., Handford, C.E., Na, J., Thomson, M., Zernicka- Goetz, M., 2020. Developmental clock and mechanism of de novo polarization of the mouse embryo. Science 370, eabd2703.

Zuo H, Lin T, Wang D, Peng R, Wang S, Gao Y, Xu X, Li Y, Wang S, Zhao L, Wang L, Zhou H. Neural cell apoptosis induced by microwave exposure through mitochondria-dependent caspase-3 pathway. Int J Med Sci. 2014 Mar 9;11(5):426-35. doi: 10.7150/ijms.6540.